Chapter V

RESULTS AND DISCUSSION

Study on *in vitro* myotoxicity (cytotoxicity towards rat myoblasts) of $NnPLA_2$-I and its acidic cognate complex on rat myotubes and their neutralization by commercial polyvalent anti-snake venom and anti-$NnPLA_2$-I antibody

Chapter V

RESULTS AND DISCUSSION: Study on *in vitro* myotoxicity (cytotoxicity towards rat myoblasts) of $NnPLA_2$-I and its acidic cognate complex on rat myotubes and their neutralization by commercial polyvalent anti-snake venom and anti-$NnPLA_2$-I antibody

5.1 Brief introduction

Phospholipase A_2 enzymes occur unambiguously in all snake venoms and exhibit a wide array of pharmacological effects by binding to target through a "pharmacological site" on the surface of the enzyme which is independent of the catalytic site [1-4]. However, the pharmacological properties of a snake venom PLA_2 enzyme may or may not be dependent on its catalytic activity [5-7].

Studies have shown that group IB mammalian $sPLA_2$s bind to PLA_2 receptor (PLA_2R), which is a transmembrane glycoprotein resembling C-type animal lectin family of receptors [8,9], to induce cell proliferation, cell migration, and production of lipid mediator(s) in mammalian cells [8,9]. Nevertheless, snake venom PLA_2s have been reported to differentially bind and attack phospholipid micro-domains or rafts present on the mammalian cells; therefore, phospholipid types in different plasma membrane of cells determines the extent of PLA_2 hydrolysis [10-12]. Studies have also revealed the presence of certain elusive PLA_2 receptors on the plasma membranes which may or may not be directly involved in the toxic effects of snake venom PLA_2s [13].

Myotoxicity is one of the major signs of cobra envenomation that results in permanent morbidities in snakebite victims [14,15]. Non-enzymatic three finger toxins (3FTxs) and enzymatically active / inactive homologs of venom PLA_2s in elapid venoms induce myotoxicity by disruption of cellular integrity of myotubes [16,17]. Catalytically inactive snake venom PLA_2s possessing Lys49, Ser49, Asn49, Glu49 or Arg49 instead of Asp49 [18] are also reported to induce myotoxicity [5,19,20].

The myotoxic PLA_2s are primarily basic in nature and their basic charge might play an important role in membrane binding and subsequent damage to the cells [21].

The present study shows that an acidic PLA_2 purified from Indian cobra *Naja naja* venom (NnV) is devoid of cytotoxicity towards myogenic cells; however, it forms a cognate complex with other components of cobra venom to show considerable cytotoxicity against rat myogenic L6 cells in *in vitro* conditions indicating PLA_2 cognate complex may play a pivotal role in cobra venom-induced cytotoxicity. The present study is also the first report showing binding of cobra venom acidic PLA_2 and its cognate complex with membrane bound vimentin of rat myogenic L6 cells to induce cytotoxicity and internalization of PLA_2 to cytosol post binding with vimentin.

5.2 Results

5.2.1 2D SDS-PAGE analysis of eastern India *N. naja* venom followed by western blot analysis to detect complex formation by $NnPLA_2$-I

The 2D SDS-PAGE of *N. naja* venom (NnV) resolved the proteins according to their mass and charge. When NnV was separated under reduced condition, it resolved into ~30 protein spots (left panel of Fig 5.1A). Immunoblot analysis showed that anti-$NnPLA_2$-I antibodies recognized only 3 spots (R1 region) of ~15 kDa mass acidic protein(s) (right panel of Fig 5.1A).

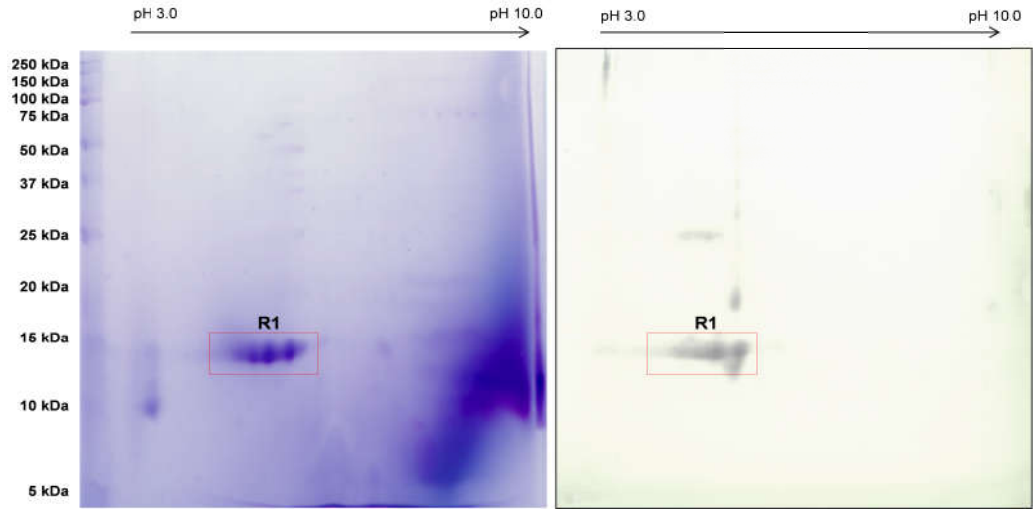

Fig 5.1A. 2D SDS-PAGE (left panel) of *N. naja* venom (300 µg) under reduced condition, and its corresponding immunoblot (right panel). The blot was developed with rabbit anti-$NnPLA_2$-I antibody (at a dilution of 1:2000) and HRP-conjugated goat anti-rabbit IgG secondary antibody (at a dilution of 1:5000).

On the other hand, separation of NnV by 2D SDS-PAGE under non-reduced condition did not resolve into specific spots, but proteins were separated as certain patches (left panel of Fig 5.1B). Immunoblot analysis demonstrated that anti-NnPLA$_2$-I antibodies recognized proteins from two broad regions R2 (20 – 24 kDa, pI 3.5 – 5.5) and R3 (22 – 37 kDa; pI 8.5 – 10) (Fig 5.1B). All the three regions (R1, R2, and R3) were subjected to LC-MS/MS analysis to determine their composition (described below, section 5.2.3).

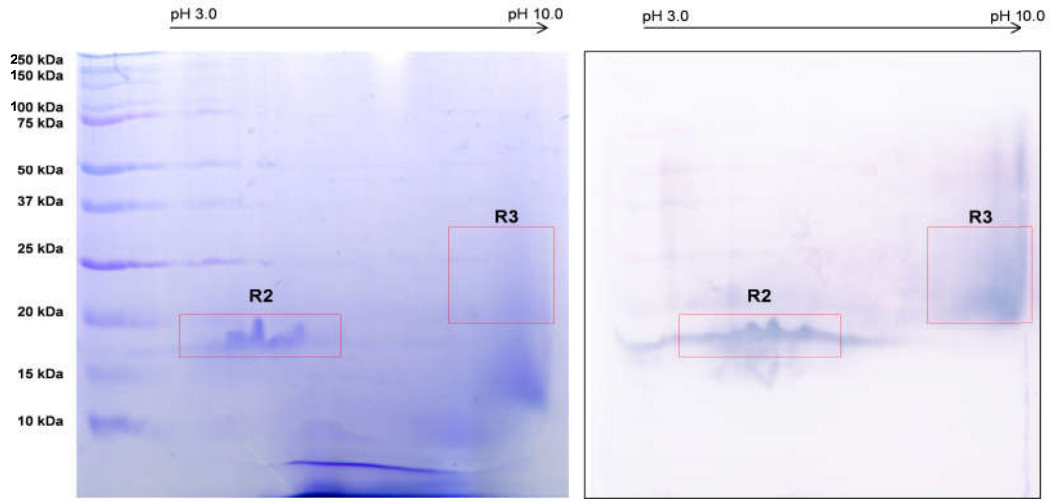

Fig 5.1B. 2D SDS-PAGE (left panel) of *N. naja* venom (300 µg) under non-reduced condition, and their corresponding immunoblot (right panel). The blot was developed with rabbit anti-NnPLA$_2$-I antibody (at a dilution of 1:2000) and HRP-conjugated goat anti-rabbit IgG secondary antibody (at a dilution of 1:5000).

5.2.2 Cation-exchange chromatography of eastern India NnV

Fractionation of crude eastern India NnV through a cation-exchange HiPrep CM FF 16/10 column (20 ml) resolved into six distinct peaks-NnCM / Nn(N)CM 1 – 6 (see Fig. 4.1A, chapter IV). The unbound or acidic fractions – Nn(N)CM1 and Nn(N)CM2 showed prominent PLA$_2$ activity of 95250 ± 3810 U/mg and 95650 ± 3826 U/mg, respectively, which were comparable to that of crude NnV (93550 ± 3742 U/mg). However, NnPLA$_2$-I was purified from Nn(N)CM1 (section 4.2.1, chapter IV) and its identity was confirmed by LC-MS/MS analysis (section 4.2.4, chapter IV). The other acidic fraction, Nn(N)CM2 was also subjected to LC-MS/MS analysis (described below, section 5.2.3) for identification of its components.

5.2.3 LC-MS/MS of Nn(N)CM2 and anti-NnPLA$_2$-I antibody recognized regions of 2D SDS-PAGE of NnV

The LC-MS/MS analyses of the three spots of R1 region (Fig 5.1A) identified the presence of isoforms of acidic PLA$_2$ enzymes (Uniprot ID P15445) (Table 5.1A), that was previously identified as NnPLA$_2$-I (Table 4.2, chapter IV). However, LC-MS/MS analysis of R2 region (Fig. 5.1B) demonstrated co-migration of isoforms of an acidic PLA$_2$ (P15445), a long chain neurotoxin (LNTx; UniProt ID P25671), a cytotoxin (CTx; UniProt ID P86538), and a venom nerve growth factor (NGF; UniProt ID P01140) from NnV with a relative abundance (RA) of 41.0%, 34.9%, 19.3%, and 4.7%, respectively (Fig 5.2A, Table 5.1B). The LC-MS/MS analysis of R3 region (Fig. 5.1B) demonstrated co-migration of LNTx (P25671; RA – 43.6%), CTxs (P86538 and P24780; RA – 20.3%), NGF (P01140; RA – 4.2%), and a cysteine rich secretory protein (UniProt ID P86543; RA – 1.6% RA) along with the isoforms of an acidic PLA$_2$ enzyme (P15445; RA – 30.3%) from NnV (Fig 5.2B, Table 5.1B).

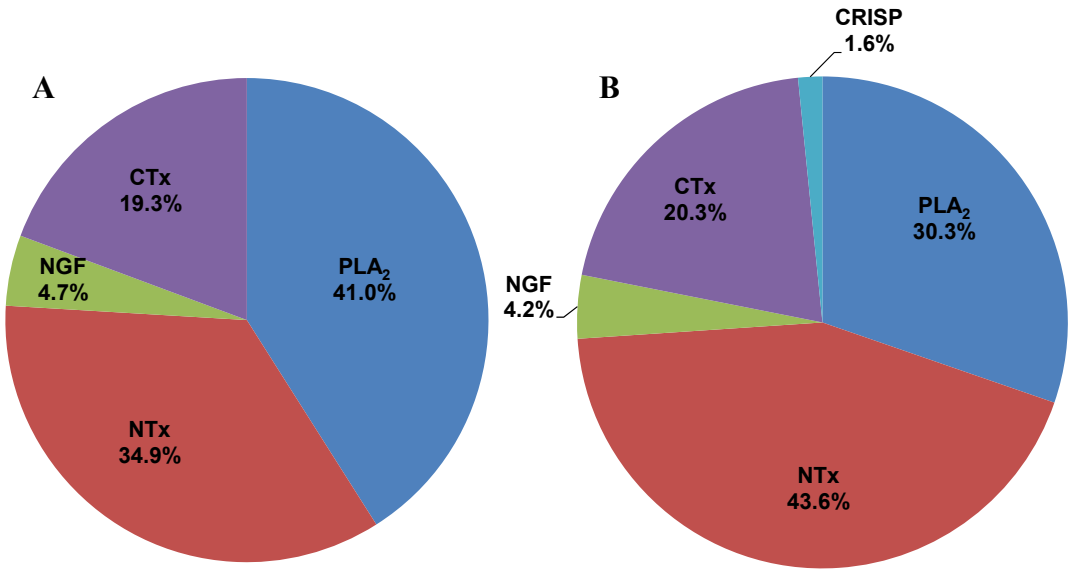

Fig 5.2. Percent relative abundances (% RA) of LC-MS/MS identified proteins in A. region 2, and B. region 3 of *N. naja* venom separated by 2D SDS-PAGE under non-reduced conditions. The % RA represents the relative composition of each component [protein: protein (w/w)] of the complex as determined by label-free MS2-based spectral count method.

The proteomic composition of Nn(N)CM2 fraction was found to consists of 38.1% PLA_2, 39.0% LNTx, 17.8% CTx, and 5.0% NGF [22] (Fig 5.2C, Table 5.2).

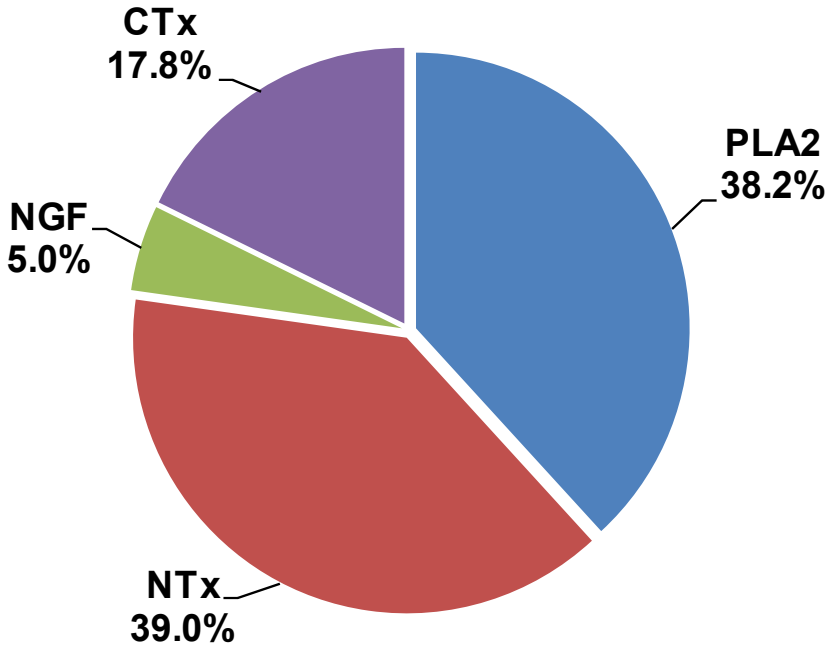

Fig 5.2C. Percent relative abundance (RA) of NnV protein/polypeptides identified by LC-MS/MS analysis of Nn(N)CM2 fraction (cognate complex). The RA was calculated by MS2-based spectral count method.

Fascinatingly, the composition as well as percent relative abundance of each toxin present in Nn(N)CM2 fraction was comparable to the composition and relative abundance of toxins of R2 region of NnV (Figs 5.2A,C, Table 5.3). Furthermore, the acidic charge of Nn(N)CM2 fraction (section 4.2.1.1, Fig 4.1A, chapter IV) correlates well with the acidic pI of R2 proteins (Fig 5.1B). Therefore, the Nn(N)CM2 fraction was considered as a cognate complex of $NnPLA_2$-I and was used for subsequent studies. Based on the percent relative abundance, it was calculated that 100 µg of Nn(N)CM2 fraction contains 38.2 µg, 39.0 µg, 17.8 µg, and 5.0 µg of PLA_2 (P15445), LNTx (P25671), CTx (P86538), and NGF (P01140), respectively.

Table 5.1A. List of identified peptides and its corresponding protein present in spot R1 of reduced 2D SDS-PAGE of *N. naja* venom by LC-MS/MS analysis. The m/z, z, assigned sequence, score for the ID, and closest homolog for the LC-MS/MS identified peptide ions obtained by analyzing the raw data using Morpheus software. The redundant peptides have been removed from the dataset. Carbamidomethylation of cysteine residue and oxidation of methionine are represented by 'c' and 'm', respectively.

Protein	Accession no.	Organism	Coverage (%)	Summed Morpheus Score	Peptide Sequence	m/z	z	Morpheus Score
Acidic phospholipase A_2 2	P15445	*Naja naja*	67.23	97.86	(R)LAAIcFAGAPYNDNNYNIDLK(A)	1179.6	2	24.1
					(R)SWWDFADYGcYcGR(G)	921.9	2	20.2
					(R)GGSGTPVDDLDR(C)	594.8	2	14.2
					(K)ISGcWPYFKTYSYEcSQGTLTcK(G)	946.5	3	1.0
					(K)NMIKcTVPSR(S)	603.9	2	2.0
					(-)NLYQFKNmIK(C)	650.4	2	2.0
					(R)ccQVHDNcYNEAEK(I)	609.9	3	2.0
					(K)GDNNAcAASVcDcDR(L)	562.4	3	2.0

Table 5.1B. List of identified peptides and its corresponding proteins present in spots R2 and R3 of non-reduced 2D SDS-PAGE of *N. naja* venom by LC-MS/MS analysis. The m/z, z, assigned sequence, score for the ID, and closest homolog for the LC-MS/MS identified peptide ions obtained by analyzing the raw data using Morpheus software. The redundant peptides have been removed from the dataset. Carbamidomethylation of cysteine residue and oxidation of methionine are represented by 'c' and 'm', respectively.

Protein Description	Accession no.	Organism	Coverage (%)	Summed Morpheus Score	Peptide Sequence	m/z	z	Morpheus Score	Spot no.
Acidic phospholipase A_2 2	P15445	*Naja naja*	67.23	117.35	(R)SWWDFADYGcYcGR(G)	921.9	2	23.3	R2,R3
					(K)TYSYEcSQGTLTcK(G)	849.4	2	23.2	
					(K)ISGcWPYFK(T)	579.3	2	13.2	
					(R)GGSGTPVDDLDRccQVHDNcYNEAEK(I)	750.0	4	9.0	
					(-)NLYQFKNMIKcTVPSR(S)	667.3	3	7.0	
					(K)GDNNAcAASVcDcDR(L)	667.3	3	7.0	
					(R)LAAIcFAGAPYNDNNYNIDLKARcQ(-)	958.1	3	3.0	
Long neurotoxin 3	P25671	*Naja naja*	60.56	60.47	(K)TGVDIQccSTDDcDPFPTR(K)	1122.0	2	16.1	R2,R3
					(K)RVDLGcAATcPTVK(T)	516.6	3	12.1	
					(-)IRCcFITPDITSKDCcPNGHVCcYTK(T)	927.5	3	2.0	
					(K)TWcDAFcSIRGKR(V)	552.4	3	1.0	
					(K)DcPNGHVccYTK(T)	450.3	3	1.0	
Venom nerve growth factor	P01140	*Naja naja*	55.17	63.33	(R)GIDSSHWNSYcTETDTFIK(A)	754.3	3	11.0	R2,R3
					(K)TTATDIKGNTVTVMENVNLDNK(V)	1190.1	2	13.0	
					(K)ALTMEGNQASWR(F)	682.3	2	12.1	
					(R)IDTAcVcVITKKTGN(-)	840.4	2	4.0	
					(K)NPNPEPSGcR(G)	564.4	2	3.0	
					(K)VYKEYFFETKcK(N)	547.7	3	2.0	

					(R)FIRIDTAcVcVITK(K)	566.0	3	1.0	
Cytotoxin 3	P24780	*Naja naja*	33.33	23.46	(K)NSLVLKYVccNTDRcN(-)	1007.5	2	3.0	R3
					(K)LIPLAYKTcPAGK(N)	716.4	2	3.0	
					(K)TcPAGKNLcYKMFMVSNK(T)	537.9	4	2.0	
					(K)MFMVSNKTVPVKR(G)	513.0	3	2.0	
					(K)RGcIDVcPKNSLVLK(Y)	440.8	4	2.0	
Cytotoxin 2a	P86538	*Naja naja*	33.33	28.45	(K)NLCcYKmFmVSDLTIPVKR(G)	563.0	4	2.0	R2,R3
					(K)MFMVSDLTIPVKRGCcIDVCcPK(N)	617.1	4	2.0	
					(K)NSLLVKYECcCcNTDRCcN(-)	682.3	3	2.0	
					(K)TCcPPGKNLCcYK(M)	446.2	3	1.0	
					(-)LQCcNKLVPIASKTCcPPGK(N)	503.0	4	1.0	
Cysteine-rich venom protein (Fragment)	P86543	*Naja naja*	30.30	12.09	(R)RRVSPTA(-)	394.7	2	2.0	R3
					(-)NVDFNSESTRRK(K)	485.3	3	2.0	
					(K)KQKEIVDLHNSLR(R)	527.3	3	1.0	
					(K)QKEIVDLHNSLRR(R)	402.9	4	1.0	

Table 5.2. List of identified proteins and their corresponding peptides by LC-MS/MS analysis of Nn(N)CM2 fraction of eastern India *N. naja* venom. The mass, m/z, z, assigned sequence, score for the ID, modified residues, and closest homolog for the LC-MS/MS identified peptide ions obtained by analyzing the raw data using PEAKS 7.0 software. The redundant peptides have been removed from the dataset. Carbamidomethylation of cysteine residue is represented by 'c'.

Protein	Accession no.	-10log P	% Coverage	Summed spectra	Homology with protein from	Distinct peptide(s)	Peptide score	m/z	z
Acidic phospholipase A_2 2	P15445	258.4	91	596	*Naja naja*	(R)GGSGTPVDDLDR(C)	62.3	594.8	2
						(-)NLYQFKN(M)	21.9	463.7	2
						(R)ccQVHDNcYNEAEK(I)	61.2	913.8	2
						(R)SWWDFADYGcYcGR(G)	60.6	921.9	2
						(K)ISGcWPYFK(T)	57.2	579.3	2
						(K)TYSYEcSQGTLTcKG(D)	54.1	877.9	2
						(K)GDNNACAASVCDCDRLAAIcFAGAPYNDNN YNIDLK(A)	20.3	1284.6	3
Cytotoxin 2a	P86538	115.1	79	56	*Naja naja*	(K)LVPIASKTCPPGK(N)	60.8	684.4	2
						(K)TCPPGKNLCYK(M)	29.4	446.5	3
						(-)LQCNKLVPIASK(T)	57.4	685.9	2
Long neurotoxin 3	P25671	199.9	97	86	*Naja naja*	(K)TWcDAFcSIRGK(R)	51.5	750.8	2
						(K)RVDLGcAATcPTVK(T)	69.7	774.4	2
Venom nerve growth factor 2	P01140	171.0	39	39	*Naja sputatrix*	(K)EYFFETK(C)	35.9	481.7	2

Table 5.3. List of proteins identified by LC-MS/MS analysis of protein spots in Nn(N)CM2, and 2D SDS-PAGE of *N. naja* venom under reduced (R1) and non-reduced (R2, R3) conditions. The protein spots were detected by immunoblot analysis against anti-$NnPLA_2$-I polyclonal antibody.

Protein Description	Accession no.	Organism	Coverage (%)	Molecular mass (Da)	Summed Morpheus Score	Unique peptides	Region/ Fraction
Acidic phospholipase A_2 2	P15445	*Naja naja*	67.23	13,346	117.35	6	R1, R2, R3, Nn(N)CM2
Long neurotoxin 3	P25671	*Naja naja*	60.56	7,833	60.47	4	R2, R3, Nn(N)CM2
Venom nerve growth factor	P01140	*Naja naja*	55.17	13,023	63.33	5	R2, R3, Nn(N)CM2
Cytotoxin 3	P24780	*Naja naja*	33.33	6,745	23.46	2	R3
Cytotoxin 2a	P86538	*Naja naja*	33.33	6,711	28.45	2	R2, R3, Nn(N)CM2
Cysteine-rich venom protein (Fragment)	P86543	*Naja naja*	30.30	3,910	12.09	1	R3

5.2.4 Determination of stoichiometry of venom proteins in the cognate complex

From the relative abundance of the components of the cognate complex, it was inferred that 100 µg of Nn(N)CM2 fraction contains 2.9 nmol, 5.0 nmol, 2.7 nmol, and 0.4 nmol of PLA_2 (P15445), LNTx (P25671), CTx (P86538), and NGF (P01140), respectively showing that the approximate molar stoichiometric ratio of PLA_2 : LNTx : CTx : NGF is 1.0 : 1.7 : 0.9 : 0.1. Considering the nearest integer, this ratio become 1:2:1 of PLA_2 : LNTx : CTx and NGF may not be a real component of the complex but an associated protein formed by non-covalent interaction with the PLA_2 cognate complex.

5.2.5 Isolation and identification of individual components of Nn(N)CM2 by RP-HPLC and LC-MS/MS analysis

RP-HPLC of Nn(N)CM2 resolved it into three major protein peaks Nn(N)CMRP1 to Nn(N)CMRP3 (Fig 5.3). The LC-MS/MS analysis of Nn(N)CM2RP1, Nn(N)CM2RP2, and Nn(N)CM2RP3 fractions resulted in their identification as LNTx (P25671), PLA_2 ($NnPLA_2$-I; P15445), and CTx (P86538), respectively (Table 5.4). However, trace amount of NGF present in the complex could not be detected by RP-HPLC.

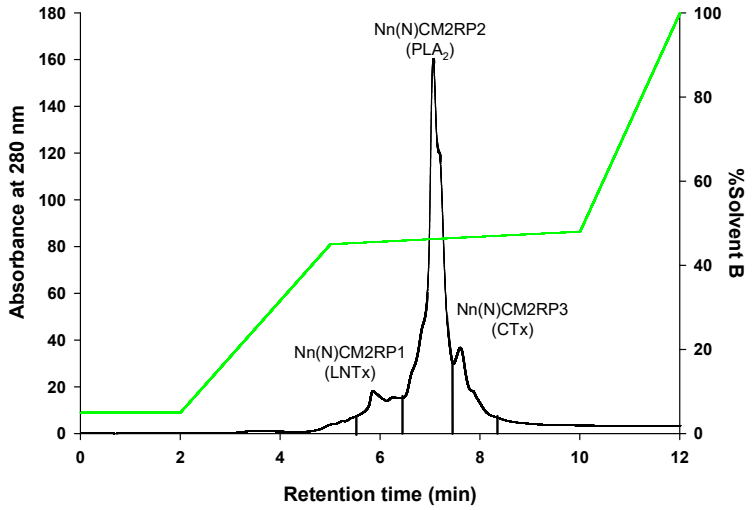

Fig 5.3. RP-HPLC of Nn(N)CM2 to isolate the individual components of the cognate complex. 150 µg of Nn(N)CM2 fraction was fractionated in a Dionex Acclaim C_{18} column (2.1 × 150 µM) pre-equilibrated with 95% solvent A (type I water containing 0.1% TFA) and 5% solvent B (90% ACN containing 0.1% TFA).

Table 5.4. LC-MS/MS analysis identified proteins and their corresponding peptides present in RP-HPLC fractions [Nn(N)CM2RP1 – 3] of Nn(N)CM2 by LC-MS/MS analysis. The m/z, z, assigned sequence, score for the ID, and closest homolog for the LC-MS/MS identified peptide ions obtained by analyzing the raw data using Morpheus software. The redundant peptides have been removed from the dataset. Carbamidomethylation of cysteine residue and oxidation of methionine are represented by 'c' and 'm', respectively.

Protein Description	Accession no.	Organism	Coverage (%)	Summed Morpheus Score	Peptide Sequence	m/z	z	Morpheus Score
Nn(N)CM2RP1								
Long neurotoxin 3	P25671	*Naja naja*	32.4	22.2	(K)TGVDIQccSTDDcDPFPTR(K)	1121.5	2	10.0
					(K)TGVDIQccSTDDcDPFPTRK(R)	791.4	3	7.0
Nn(N)CM2RP2								
Acidic phospholipase A_2 2	P15445	*Naja naja*	55.5	60.6	(K)ISGcWPYFK(T)	579.3	2	10.1
					(K)TYSYEcSQGTLTcK(G)	849.3	2	7.1
					(-)NLYQFKNmIKcTVPSR(S)	672.0	3	3.0
					(R)LAAIcFAGAPYNDNNYNIDLKARcQ(-)	1437.2	2	3.0
					(K)GDNNAcAASVcDcDR(L)	562.4	3	2.0
					(C)cTVPSR(S)	359.2	2	1.1
					(R)SWWDFADYGcYcGRGGSGTPVDDLDR(C)	430.9	7	1.0
Nn(N)CM2RP3								
Cytotoxin 2a	P86538	*Naja naja*	45.0	53.4	(K)MFMVSDLTIPVKR(G)	512.9	3	11.1
					(K)MFMVSDLTIPVKRGCIDVCPK(N)	617.1	4	4.0
					(K)MFMVSDLTIPVK(R)	460.5	3	3.0
					(K)LVPIASKTCPPGK(N)	683.4	2	20.1

5.2.6 One-dimensional SDS-PAGE analysis of Nn(N)CM2

The SDS-PAGE analysis of Nn(N)CM2 fraction under reduced conditions showed two prominent protein bands at 5 – 7 kDa and ~15 kDa regions (Fig 5.4). Nevertheless, under non-reduced conditions this fraction showed a broad aggregated protein band in the molecular mass range of 14 – 37 kDa (Fig 5.4) which is much higher as compared to the molecular weight of R2 region of non-reduced 2D SDS-PAGE of NnV (Fig 5.1B). Snake venom proteins are known to form higher mass aggregates when stored in solution [23] and this may be the reason for which the molecular mass range of $NnPLA_2$-I-cognate complex was found to be higher by 1D SDS-PAGE analysis (Fig 5.4). The $NnPLA_2$-I under reduced and non-reduced conditions showed a sharp and diffused band of ~15 kDa, respectively (Fig 5.4).

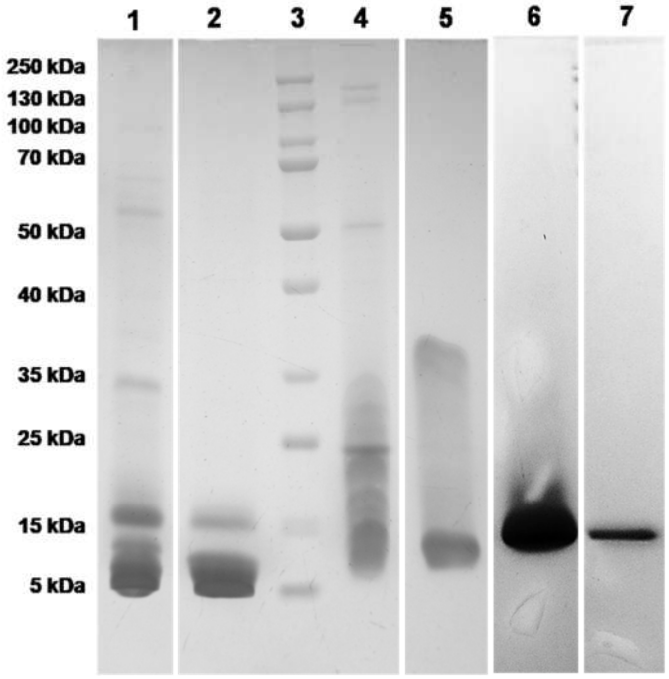

Fig 5.4. 12.5% SDS-PAGE analysis of $NnPLA_2$-I and its cognate complex [Nn(N)CM2 fraction] under reduced and non-reduced conditions. Lanes 1 – 2, *N. naja* venom (50 µg) and $NnPLA_2$-I cognate complex (30 µg), respectively separated under reduced conditions; lane 3, protein molecular markers; lanes 4 – 5, *N. naja* venom (50 µg) and $NnPLA_2$-I cognate complex (30 µg) separated under non-reduced conditions, respectively; lanes 6 – 7, non-reduced and reduced $NnPLA_2$-I (30 µg), respectively.

5.2.7 Determination of molecular mass of Nn(N)CM2 by gel filtration chromatography

Size exclusion chromatography (SEC) of Nn(N)CM2 demonstrated the elution of cognate complex as a single prominent broad peak from 49.8 to 62.0 ml with the highest intensity at 59.8 ml (Fig 5.5A) which corresponds to molecular mass of the cognate complex in the range of 22 – 39.8 kDa (Fig 5.5B). This data corroborates with the molecular mass of the cognate complex determined by 1D SDS-PAGE analysis of Nn(N)CM2 under non-reduced conditions (Fig 5.4).

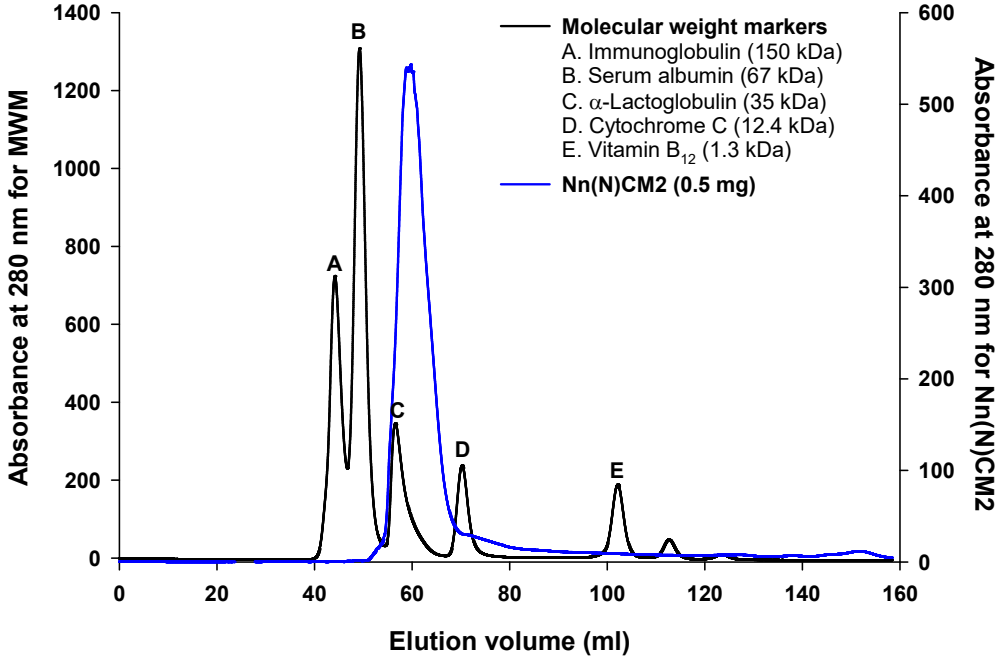

Fig 5.5A. Gel filtration chromatography of Nn(N)CM2 to determine the molecular mass range of the $NnPLA_2$-I cognate complex. The Nn(N)CM2 (0.5 mg) was fractionated through a HiLoad 16/600 Superdex 75 pg column (120 ml), pre-equilibrated with 20 mM Tris-HCl containing 150 mM NaCl, pH 7.4, coupled to an AKTA Purifier FPLC System.

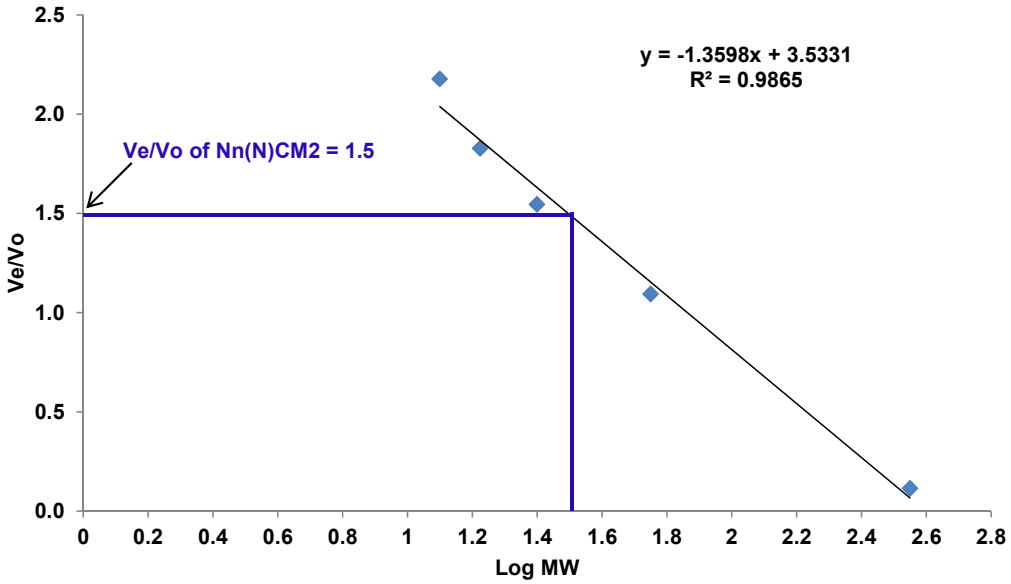

Fig 5.5B. Log (base 10) molecular weight of protein molecular markers vs Ve/Vo (Ve = elution volume of marker proteins; Vo = void volume of column) **plot** to determine the molecular mass of $NnPLA_2$-I cognate complex [Nn(N)CM2]. Molecular weight markers: A, Immunoglobulin (150 kDa); B, Serum albumin (67 kDa); C, α-Lactoglobulin (35 kDa); D, cytochrome C (12.4 kDa); E, Vitamin B_{12} (1.3 kDa).

Taken together, LC-MS/MS, 1D SDS-PAGE, and SEC of Nn(N)CM2 fraction demonstrated that the components of the cognate complex (PLA_2 : LNTx : CTx) exist in a stoichiometric ratio of 1:2:1 which corresponds to molecular mass of the cognate complex at ~36 kDa. The RP-HPLC analysis did not show NGF peak (Fig 5.3), albeit LC-MS/MS analysis suggested presence of trace amount of NGF in this complex which reinstates that NGF may not be a real component of this complex.

5.2.8. Quantitation of $NnPLA_2$-I in Nn(N)CM2 by ELISA

The recognition of different concentrations of $NnPLA_2$-I (0.17 µM, 0.35 µM and 0.70 µM) and Nn(N)CM2 (6.25 µg/ml, 12.5 µg/ml and 25.0 µg/ml) was done by anti-$NnPLA_2$-I using ELISA. The different concentrations of $NnPLA_2$-I were calculated on the basis of percent relative abundance obtained from LC-MS/MS analysis of Nn(N)CM2 by MS2-based spectral count (sections 5.2.3 and 5.2.4). Quantitative analysis of the ELISA results demontrated that 6.25 µg/ml, 12.5 µg/ml and 25.0 µg/ml

of $NnPLA_2$-I cognate complex [Nn(N)CM2] consists of approximately 0.17 µM, 0.35 µM and 0.70 µM of $NnPLA_2$-I, respectively (Fig 5.6).

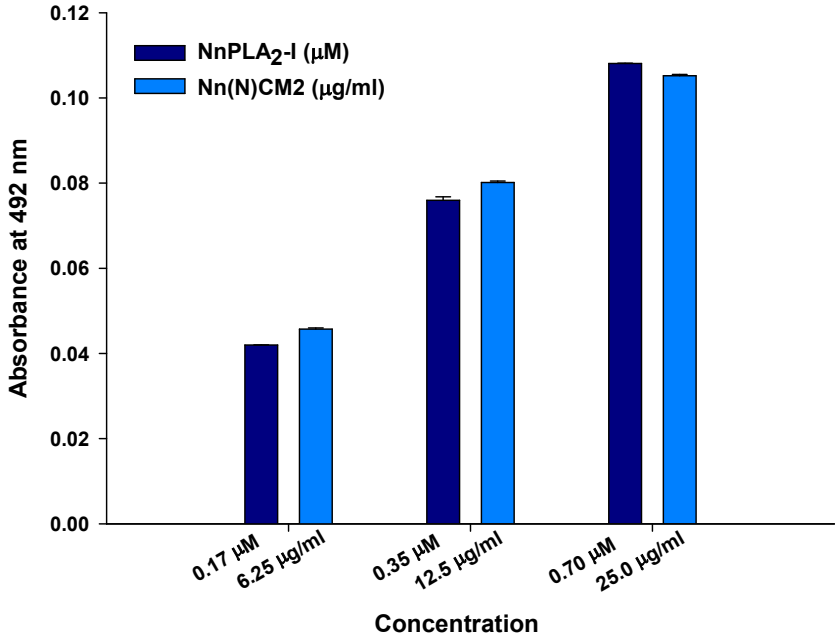

Fig 5.6. ELISA to quantitate the $NnPLA_2$-I in Nn(N)CM2 fraction (cognate complex) **by anti-$NnPLA_2$-I antibodies.** Quantitative analysis was done by comparing the absorbance of different concentrations of $NnPLA_2$-I (0.17, 0.35 and 0.70 µM) with that of Nn(N)CM2 (6.25, 12.5 and 25.0 µg/ml). Values are mean ± SD of triplicate determinations.

5.2.9 Cytotoxicity of PLA_2 and its cognate complex against the mammalian and bacterial cells

The cytotoxicity exhibited by $NnPLA_2$-I (10.0 µg/ml or 0.70 µM) and two different doses of cognate complex [12.5 and 25.0 µg/ml of cognate complex containing 5.0 µg/ml or 0.35 µM and 10.0 µg/ml or 0.70 µM of $NnPLA_2$-I, respectively as determined by LC-MS/MS (Fig 5.2C) and ELISA (Fig 5.6)] is shown in Fig 5.7A. The $NnPLA_2$-I-cognate complex exhibited cytotoxicity against the mammalian cells in the following order – L6 myoblasts>platelets>PC12 (Fig 5.7A). The $NnPLA_2$-I and its cognate complex did not demonstrate cytotoxicity against erythrocytes, MCF-7, and HEK-29 cells or antibacterial activity against *B. subtilis* and *E. coli* cells (Fig 5.7A).

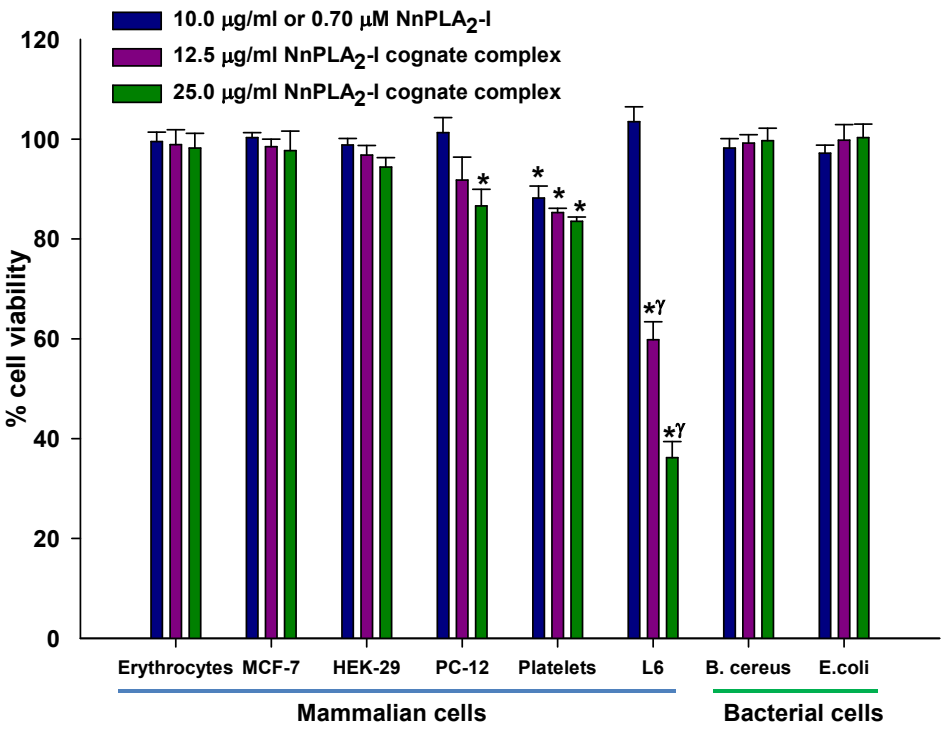

Fig 5.7A. Determination of cytotoxicity of $NnPLA_2$-I and its cognate complex [Nn(N)CM2] post 24 h of incubation against different mammalian and bacterial cells. The L6 cells used for the assay were partially differentiated myoblasts. Values are mean ± SD of three experiments. Significance of difference *$p<0.05$ and $^{\gamma}p<0.05$ as compared to control and 10.0 µg/ml $NnPLA_2$-I induced toxicity, respectively.

5.2.10 Assessment of release of creatine kinase and lactate dehydrogenase from $NnPLA_2$-I cognate complex treated L6 myoblasts

The $NnPLA_2$-I cognate complex showed highest toxicity against myoblasts which was also confirmed by measuring the enhanced release of CK and LDH from the treated cells compared to control cells. The $NnPLA_2$-I had no effect on release of these enzymes albeit $NnPLA_2$-I-cognate complex significantly enhanced the release of CK and LDH from myoblasts to the culture media (Table 5.5).

Table 5.5. Release of creatine kinase (CK) and lactate dehydrogenase (LDH) enzymes in the culture media of L6 cells (myoblasts) treated with $NnPLA_2$-I (10.0 µg/ml or 0.70 µM)**, $NnPLA_2$-I cognate complex [Nn(N)CM2]** (12.5 µg/ml containing 0.35 µM of $NnPLA_2$-I)**, and crude *N. naja* venom** (45.0 µg/ml containing 0.35 µM of

$NnPLA_2$-I). Values are mean ± SD of triplicate determinations. Significance of difference with respect to control, *p<0.05.

Samples	**CK (U/dL)**	**LDH (U/dL)**
Control	9.5 ± 0.29	46.3 ± 1.39
$NnPLA_2$-I (10.0 µg/ml)	10.2 ± 0.31	50.2 ± 1.51
$NnPLA_2$-I cognate complex (12.5 µg/ml)	28.9 ± 0.27*	102.7 ± 1.08*
N. naja venom (45.0 µg/ml)	32.3 ± 0.67*	128.6 ± 2.86*
Triton X-100	56.3 ± 0.69*	190.5 ± 3.72*

5.2.11 Cytotoxicity of $NnPLA_2$-I cognate complex and its individual components on rat myoblasts

5.2.11.1 Determination of cytotoxicity by MTT assay

The cytotoxicity exhibited by the native cognate complex was found to be significantly higher as compared to the individual components of this complex ($NnPLA_2$-I, LNTx, and CTx), re-constituted CTx-LNTx complex and re-constituted CTx-LNTx-PLA_2 complex (Table 5.6). However, non-covalent interaction of $NnPLA_2$-I with basic proteins of NnV to form a cognate complex did not result in increase in its catalytic activity (Table 5.6). Furthermore, pre-incubation of $NnPLA_2$-I-cognate complex with PAV, anti-$NnPLA_2$-I antibody, and *p*-BPB (inhibitor of histidine) resulted in a significant reduction of its cytotoxicity against rat myoblasts; PAV was more effective in reducing the cytotoxicity of $NnPLA_2$-I-cognate complex whereas anti-$NnPLA_2$-I antibody showed higher inhibition of PLA_2 activity of the cognate complex (Table 5.6). Treatment with *p*-BPB resulted in a significant reduction of the catalytic activity and cytotoxic property of the $NnPLA_2$-I cognate complex (Table 5.6). However, addition of PAV to L6 myotube culture medium post 60 – 240 min of treatment with $NnPLA_2$-I cognate complex resulted in a gradual loss of its cytotoxic property (Table 5.6).

Table 5.6. A comparison of the cytotoxicity exhibited by the individual components of the complex, and neutralization or inhibition of PLA_2 activity and cytotoxicity of $NnPLA_2$-I cognate complex by commercial polyvalent antivenom (PAV), anti-$NnPLA_2$-I antibodies and *p*-bromophenacyl bromide (*p*-BPB) towards L6 myogenic cells. Cytotoxicity was measured by MTT-based assay**.** Values are mean ± SD of triplicate determinations. Significance of difference with respect to cognate complex *p<0.05, **p<0.01, and with respect to PAV treated cognate complex ¶p<0.05.

Sample	Cognate complex: Ab	Residual activity	
		PLA_2 activity (Unit)[a]	Cytotoxicity (% cell death)
$NnPLA_2$-I (0.70 µM)	-	94.8 ± 1.2	0.0
CTx (0.35 µM)	-	-	14.7 ± 0.08**
LNTx (0.62 µM)	-	-	6.1 ± 0.05**
Re-constituted CTx-LNTx complex	-	-	16.5 ± 0.15**
Re-constituted CTx-LNTx-PLA_2 complex	-	93.9 ± 0.8	31.8 ± 0.09*
Cognate complex (12.5 µg/ml)	-	93.6 ± 0.13	40.9 ± 0.08
Cognate complex pre-incubated with anti-$NnPLA_2$-I Ab	1:25	5.2 ± 0.11**¶	16.7 ± 0.12*¶
Cognate complex pre-incubated with 5 mM *p*-BPB	-	3.5 ± 0.10**	10.5 ± 0.10**
Cognate complex pre-incubated with PAV	1:6.25	74.2 ± 0.33*	22.7 ± 0.18*
	1:12.5	41.2 ± 0.21*	9.2 ± 0.10**
	1:25	25.8 ± 0.30**	3.2 ± 0.10**

Cognate complex treatment (60 min) + PAV	1:25	-	25.6 ± 1.73*
Cognate complex treatment (120 min) + PAV		-	31.5 ± 2.43
Cognate complex treatment (240 min) + PAV		-	35.1 ± 1.95

[a]One Unit of PLA_2 activity is defined as decrease in 0.01 absorbance of the reaction mixture in 10 min at 740 nm. The cytotoxicity was determined by MTT-based assay.

5.2.11.2 Determination of cytotoxicity by bright field microscopy

The $NnPLA_2$-I-cognate complex-induced cytotoxicity towards L6 myoblasts was also evident from the bright field microscopic observation of the treated cells (Figs 5.7B, C). The L6 myoblasts were allowed to slightly differentiate to spindle shaped elongated myoblasts before treatment (Fig 5.7Bi, ii). As compared to the myoblasts treated with the individual toxins ($NnPLA_2$-I, CTx, and LNTx) of the complex (Fig 5.7Biii, iv, v) or re-constituted CTx-LNTx complex (Fig 5.7Bvi), the myoblasts treated with reconstituted CTx-LNTx-$NnPLA_2$-I complex (Fig 5.7Bvii) or $NnPLA_2$-I native cognate complex (Fig 5.7Bviii) demonstrated significant decrease in cell number (cytotoxicity) and changes in the cellular morphology (marked with red arrows).

In addition to cytotoxicity, the myoblasts treated with reconstituted 3FTx-$NnPLA_2$-I complex (Fig 5.7Bvii) and native cognate complex (Fig 5.7Bviii) showed loss of well distended structure of the partially differentiated myoblasts (shown with arrows); albeit the latter showed significantly higher toxicity than that of the former. The higher toxicity of cognate complex compared to reconstituted complex (devoid of NGF) suggests that NGF present in the native cognate complex contributes to the cytotoxic property of this complex. Pre-incubation of $NnPLA_2$-I-cognate complex with anti-$NnPLA_2$-I antibodies (Fig 5.7Bix) or 5 mM *p*-BPB (Fig 5.7Bx) significantly inhibited its cytotoxic property.

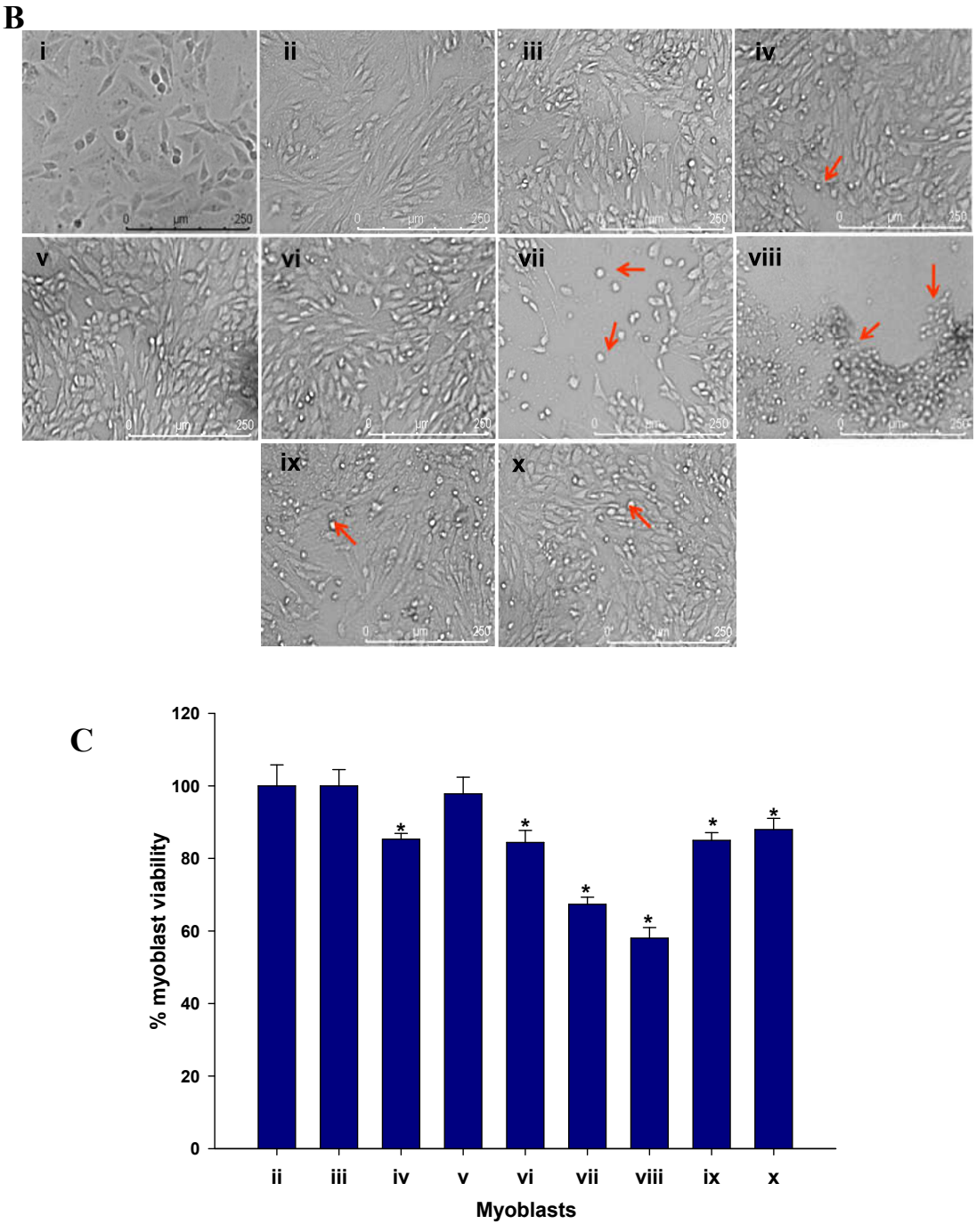

Fig 5.7B. Bright field microscopy (10 X) for determination of cytotoxicity of $NnPLA_2$-I cognate complex and its individual components against partially differentiated rat myoblasts. The micrographs were taken at 10 X magnification (scale bar = 250 µm). **(i)** undifferentiated myoblasts; partially differentiated myoblasts treated with **(ii)** PBS (control), **(iii)** $NnPLA_2$-I (10.0 µg/ml or 0.70 µM), **(iv)** CTx (2.2 µg/ml or 0.35 µM), **(v)** LNTx (4.8 µg/ml or 0.62 µM), **(vi)** reconstituted CTx (0.35 µM)-LNTx (0.62 µM) complex, **(vii)** reconstituted CTx (0.35 µM)-LNTx (0.62 µM)-$NnPLA_2$-I

(0.35 µM) complex, **(viii)** native $NnPLA_2$-I cognate complex (12.5 µg/ml), **(ix)** $NnPLA_2$-I cognate complex (12.5 µg/ml) pre-incubated with anti-$NnPLA_2$-I antibodies at 1: 25 ratio, **(x)** $NnPLA_2$-I cognate complex (12.5 µg/ml) pre-incubated with 5.0 mM *p*-BPB. The red arrows show dead cells with changed morphology. **C. Percent cell viability determined from cell count analysis of the bright field images [Fig 5.7B(ii-x)] of untreated and treated myoblasts.** Fig 5.7B(i) corresponds to undifferentiated myoblasts and hence not considered for this analysis. Values are mean ± SD of three experiments. Significance of difference *$p<0.05$ and $^{\gamma}p<0.05$ as compared to control and 12.5 µg/ml $NnPLA_2$-I cognate complex-induced cytoxicity, respectively.

5.2.11.3 Determination of cytotoxicity by acridine orange / ethidium bromide staining

The fluorescent microscopic observation of $NnPLA_2$-I-cognate complex treated myoblasts after acridine orange and ethidium bromide (AO / EB) staining showed dead nuclei stained red with dispersed nuclear matter (Fig 5.7D) due to disintegration of nuclei.

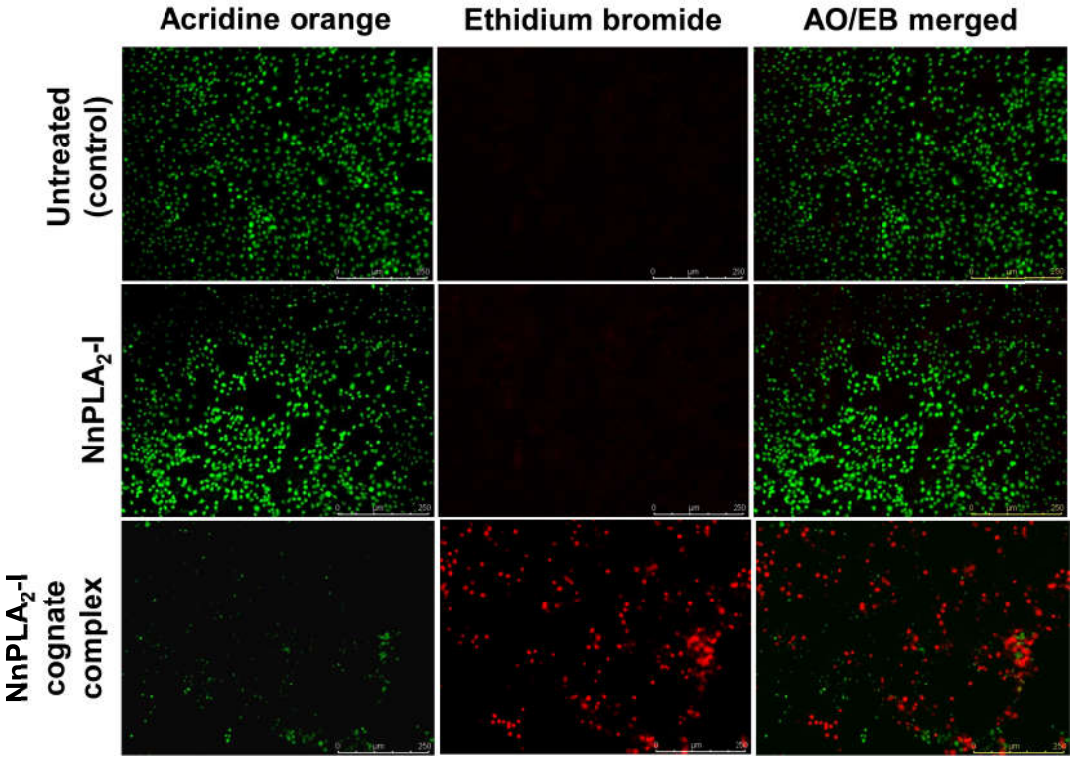

Fig 5.7D. Fluorescent microscopic images (10 X) of AO / EB stained partially differentiated L6 myoblasts treated with PBS (control), $NnPLA_2$-I (10.0 µg/ml or

0.70 µM), and NnPLA$_2$-I cognate complex (12.5 µg/ml). The green color shows live cell nuclei whereas red color shows dead nuclei of treated cells.

5.2.12 ELISA to determine binding of NnPLA$_2$-I to rat myoblasts

It was found that NnPLA$_2$-I alone and in association with other basic proteins of NnV (cognate complex) binds to L6 myoblasts; however, in cognate complex form it showed significantly higher binding ($p<0.05$) compared to binding of individual NnPLA$_2$-I (Fig 5.8).

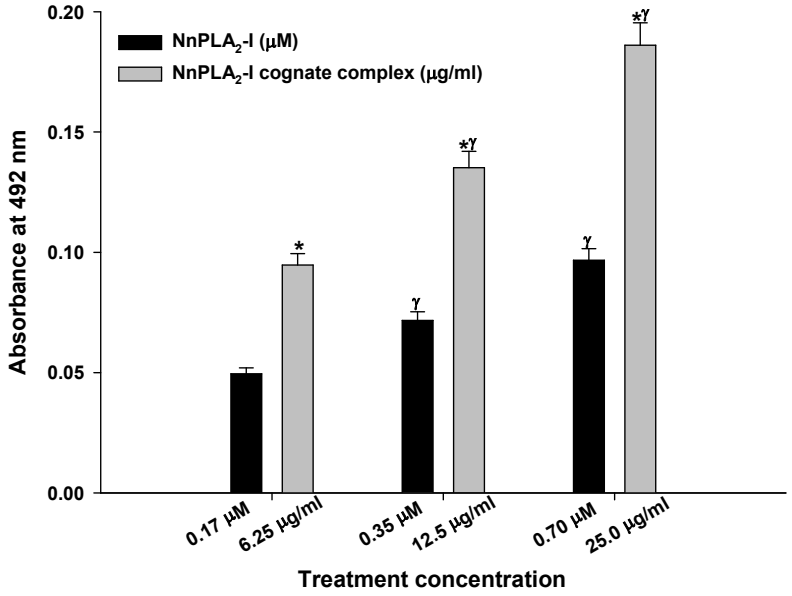

Fig 5.8. Dose-dependent binding of NnPLA$_2$-I (0.17 – 0.70 µM) and its cognate complex (6.25 – 25.0 µg/ml) to L6 myoblasts. The binding was determined by ELISA using anti-NnPLA$_2$-I antibodies and HRP conjugated goat anti-rabbit IgG. Values are mean ± SD of triplicate determinations. Significance of difference *$p<0.05$ with respect to NnPLA$_2$-I, and $^{\gamma}p<0.05$ as compared to the cognate complex (6.25 µg/ml).

5.2.13 Time-dependent internalization of NnPLA$_2$-I in rat myoblasts

5.2.13.1 Fluorescence microscopy to determine internalization of NnPLA$_2$-I

Time-dependent (30, 60, 120, and 240 min) incubation of partially differentiated rat myoblasts with 10.0 µg/ml or 0.70 µM of NnPLA$_2$-I followed by fluorescent staining using Alexa Fluor 488 conjugated to secondary antibody against rabbit IgG and

DAPI (described in section 3.2.11.2, chapter III) demonstrated binding followed by time-dependent internalization of $NnPLA_2$-I in myoblasts (Fig 5.9A).

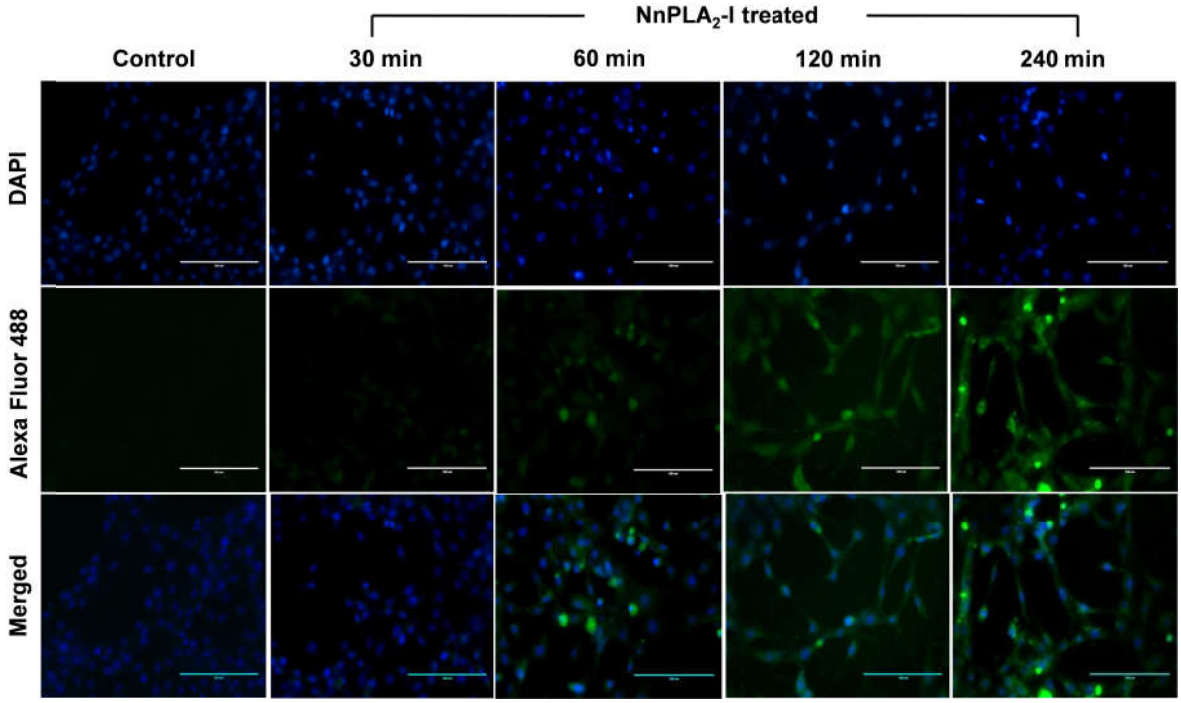

Fig 5.9A. Fluorescence microscopic images (40 X) showing time-dependent (30 – 240 min) internalization of $NnPLA_2$-I (10.0 µg/ml or 0.70 µM) in L6 rat myoblasts. The $NnPLA_2$-I was detected using rabbit anti-$NnPLA_2$-I antibody. The green images are due to Alexa fluor 488 conjugated anti-rabbit IgG (secondary antibody) visualized under FITC filter whereas blue images for nuclear staining by DAPI were visualized under DAPI filter. Scale bar = 100 µm.

5.2.13.2 Confocal microscopy to determine internalization of FITC-conjugated $NnPLA_2$-I

Observation under a confocal microscope confirmed the time-dependent internalization of FITC-conjugated $NnPLA_2$-I (Fig 5.9B). The Z-stack analysis of each image, which has been used for deconvolution of confocal microscopy data, demonstrated localization of $NnPLA_2$-I (green colour) in the cytoplasm of the myogenic cells (Fig 5.9C).

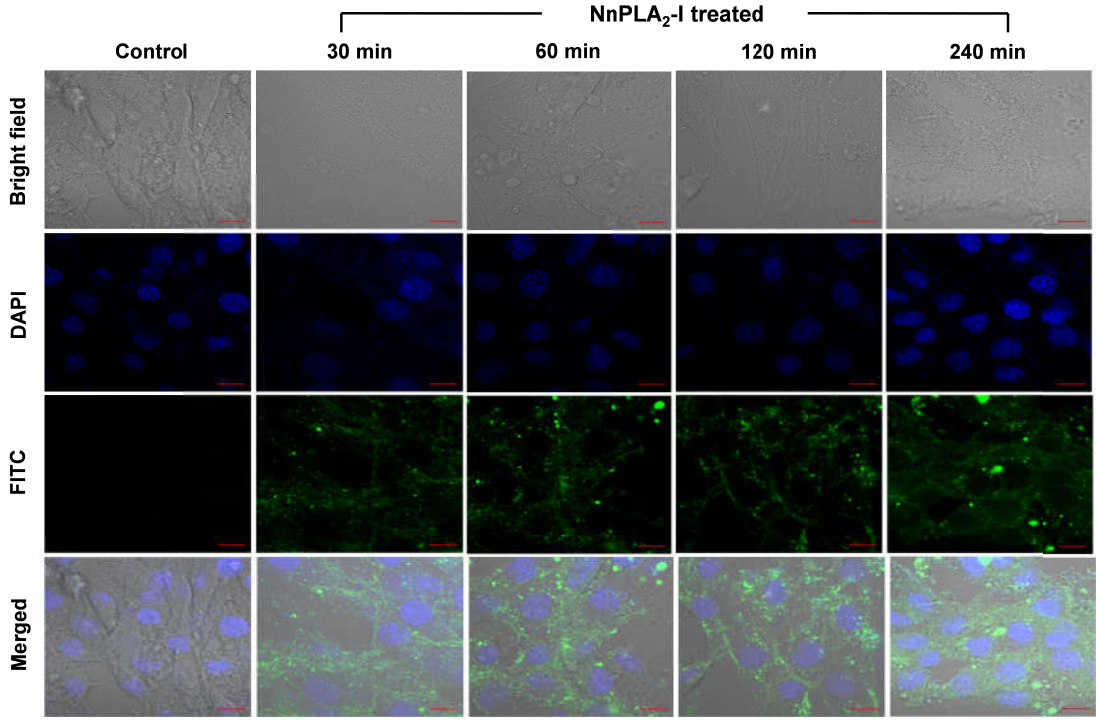

Fig 5.9B. Confocal microscopic images (63 X magnification) showing time-dependent internalization of FITC-conjugated NnPLA$_2$-I (10.0 µg/ml or 0.70 µM) after 30 – 240 min incubation with L6 myoblasts. Green (for NnPLA$_2$-I) and blue (for nucleus) images were visualized under FITC and DAPI filters, respectively. Bar scale = 10 µM.

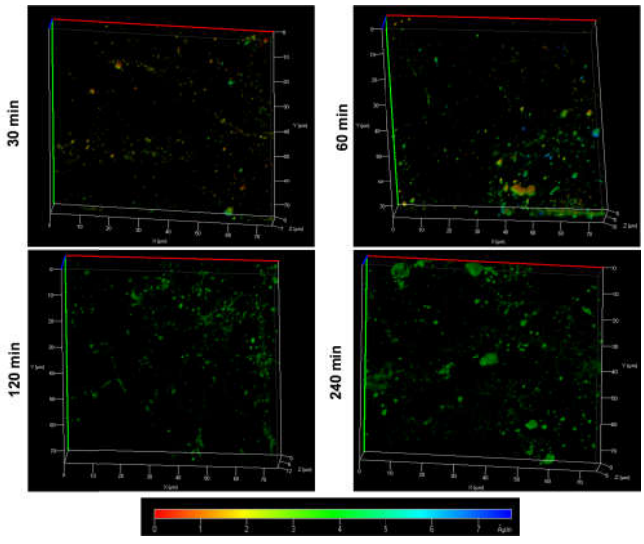

Fig 5.9C. Z-stack projection analysis to determine the time-dependent internalization of NnPLA$_2$-I in rat myoblasts. The scale (10 µm) represents the distance of the protein from the coverslip. The red colour represents that the protein is

binding only to the surface of the cells, while blue colour represents maximum penetration of the protein in the cytoplasm.

5.2.14 Binding of $NnPLA_2$-I and its cognate complex to rat myoblast membrane proteins (L6MP)

5.2.14.1 ELISA showed binding of $NnPLA_2$-I and its cognate complex to L6MP

The ELISA revealed the binding of $NnPLA_2$-I and its cognate complex to rat L6 myoblasts membrane proteins (L6MP) albeit they showed insignificant binding to cytosolic proteins (L6CP) of the same cells (Fig 5.10).

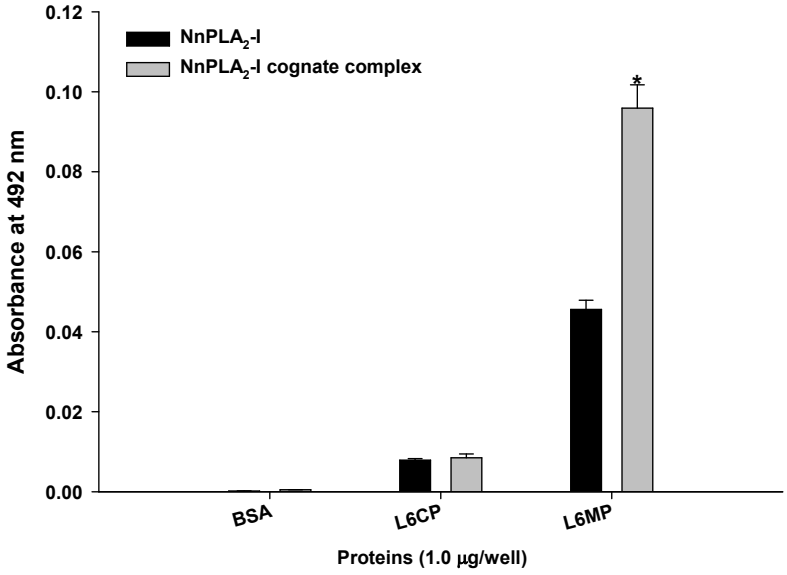

Fig 5.10. ELISA to determine the binding of $NnPLA_2$-I (10.0 µg/ml or 0.70 µM) and $NnPLA_2$-I in its cognate complex [25.0 µg/ml containing 10.0 µg/ml (0.70 µM) $NnPLA_2$-I] to L6CP, L6MP, and BSA (negative control). The binding was detected using rabbit anti-$NnPLA_2$-I antibodies (primary antibody) and HRP-conjugated anti-rabbit IgG (secondary antibodies). Values are mean ± SD of triplicate determinations. Significance of difference with respect to binding of $NnPLA_2$-I, *$p<0.05$.

5.2.14.2 Immunoblot analysis confirmed binding of $NnPLA_2$-I and its cognate complex to L6MP

L6MP and L6CP resolved into several protein bands when subjected to 12.5% SDS-PAGE analysis (left panel of Fig 5.11A). The $NnPLA_2$-I in its cognate complex

showed significantly higher binding ($p<0.05$) to L6MPs compared to individual $NnPLA_2$-I (right panel of Fig 5.11A). Immunoblot analysis indicated binding of $NnPLA_2$-I to ~55 kDa and to a lesser extent ~48 kDa L6MP (Figs 5.11A,B) and this binding was significantly enhanced when the $NnPLA_2$-I was in its cognate complex with other proteins of NnV (Figs 5.11A,B). However, we could not detect the binding of $NnPLA_2$-I and its cognate complex to L6CP (Figs 5.11A,B) by immunoblot analysis. Immunoblot analysis also demonstrated binding of $NnPLA_2$-I cognate complex with a L6MP protein band of ~40 kDa (lane 7, right panel of Fig 5.11A). Because no corresponding band was detected in lane 6 (L6MP incubated with $NnPLA_2$-I), therefore, this band was not considered for further analysis.

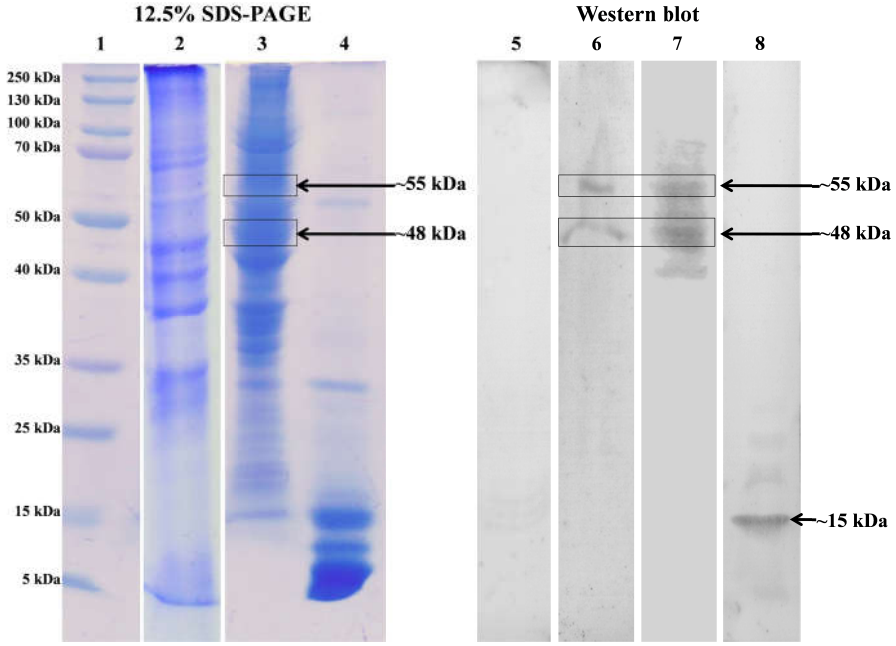

Fig 5.11A. Immunoblot analysis to detect binding of $NnPLA_2$-I and its cognate complex to membrane proteins of rat myoblasts (L6MP). Left panel: 12.5% SDS-PAGE of 80 µg each of non-reduced L6CP (lane 2), non-reduced L6MP (lane 3), and reduced NnV (lane 4). Lane 1, protein molecular markers. **Right panel:** Western blot of L6CP incubated with 25.0 µg/ml of $NnPLA_2$-I cognate complex (containing 10.0 µg/ml or 0.70 µM $NnPLA_2$-I) (lane 5), L6MP incubated with 0.70 µM $NnPLA_2$-I (lane 6), L6MP incubated with 25.0 µg/ml cognate complex (lane 7), NnV (lane 8, positive control). The binding of $NnPLA_2$-I and its cognate complex to L6MP was detected by anti-$NnPLA_2$-I antibodies.

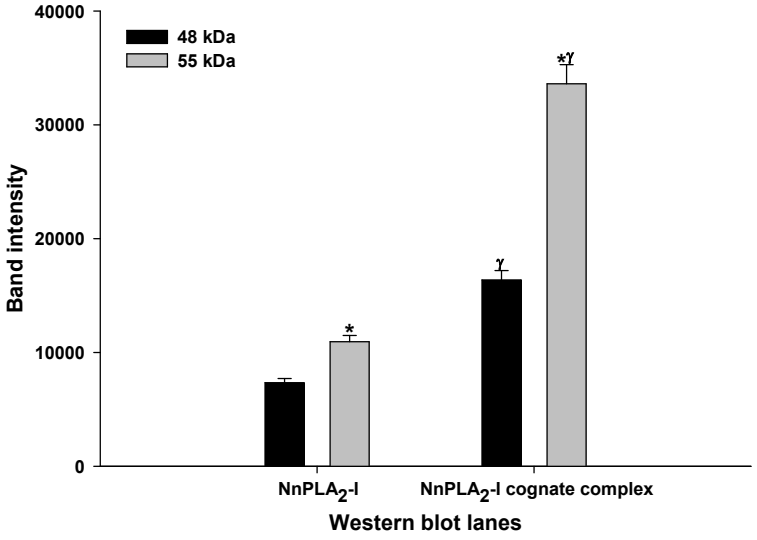

Fig 5.11B. Densitometry analysis of ~48 kDa and ~55 kDa L6MPs showing interaction with NnPLA$_2$-I / cognate complex. Values are mean ± SD of triplicate determinations. Significance of difference *p<0.05 with respect to 48 kDa band intensity; $^{\gamma}$p<0.05 as compared to binding by NnPLA$_2$-I.

5.2.15 RP-HPLC of affinity purified L6MP

NnPLA$_2$-I binding L6MP was purified by affinity purification using NnPLA$_2$-I as a ligand (described in chapter III, section 3.2.12.3.1). Thereafter, RP-HPLC of NnPLA$_2$-I-bound L6MP resolved into one major peak (L6RP1) and four minor peaks (L6RP2-L6RP5) (Fig 5.12).

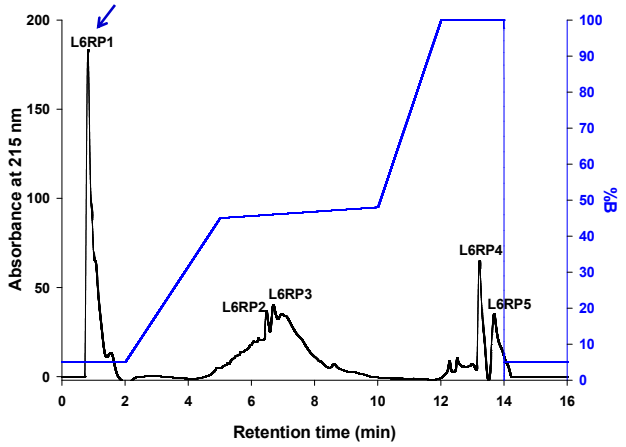

Fig 5.12. RP-HPLC fractionation of affinity purified NnPLA$_2$-I (ligand) bound L6MP. The fractionation was done in a Dionex Acclaim C_{18} column (2.1 × 150 mm, 3

µm) coupled to an UHPLC system. The column was pre-equilibrated with 95% solvent A (0.1% tri-fluoroacetic acid) and the bound proteins were eluted with a multi-step gradient of solvent B (90% acetonitrile containing 0.1% TFA). The flow rate was maintained as 0.5 ml/min.

5.2.16. ELISA to determine the binding of NnPLA$_2$-I to L6RP1

ELISA demonstrated binding of NnPLA$_2$-I with the major protein peak L6RP1 (Fig 5.13). The binding was detected using anti-NnPLA$_2$-I antibodies.

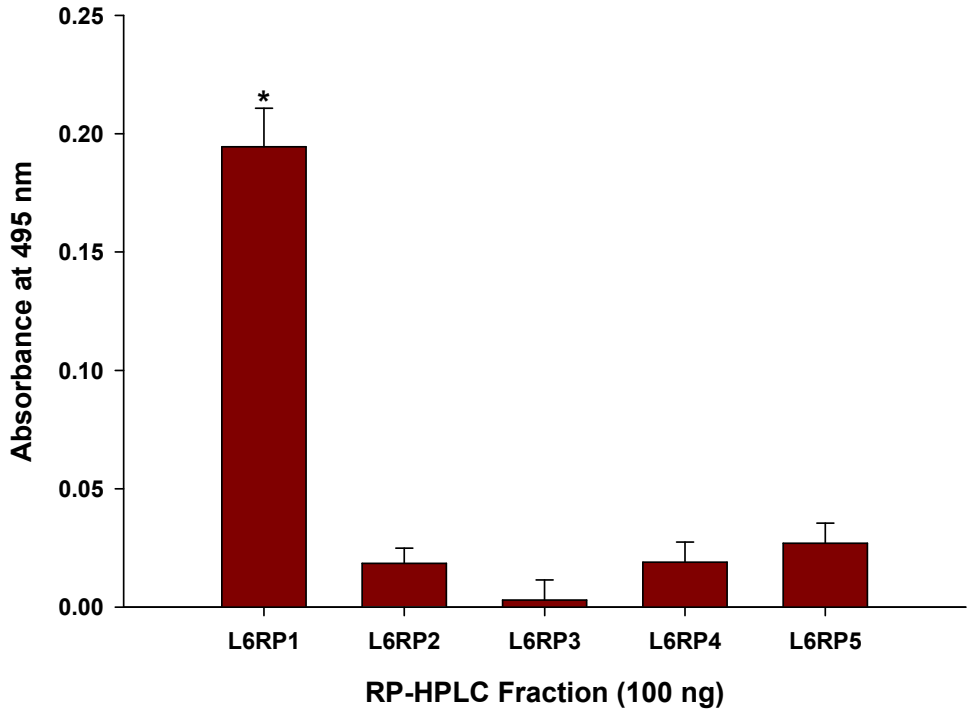

Fig 5.13. ELISA showing binding of NnPLA$_2$-I (10.0 µg/ml or 0.70 µM) to L6RP1 (100 ng). The binding was detected using anti-NnPLA$_2$-I antibodies (1:2000 dilution, primary antibody) and HRP-conjugated anti-rabbit IgG (secondary antibody). Values are mean ± SD of triplicate determinations. Significance of difference *$p<0.05$ with respect to all other L6RP fractions (L6RP2-5).

5.2.17 Identification of NnPLA$_2$-I binding L6MP by LC-MS/MS analysis

The LC-MS/MS analysis of ~48 kDa and ~55 kDa membrane protein bands showing binding with Nn-PLA$_2$-I and its cognate complex demonstrated highest resemblance with vimentin (M_r = 53.5 kDa) from *Rattus norvegicus* (UniProt ID

P31000), an intermediate filament of the cytoskeletal (Table 5.7). Tandem mass spectrometry analysis of ~48 kDa protein demonstrated a truncated vimentin where its 20 amino acid residues (~5.4 kDa) from N-terminal region (head-region) were found to be missing. Strikingly, the ~48 kDa L6MP band primarily comprised of tubulin α3 (40%), tubulin β5 (12%) chains of myotubes cytoskeleton, and vimentin (5.3%) (Fig 5.14A).

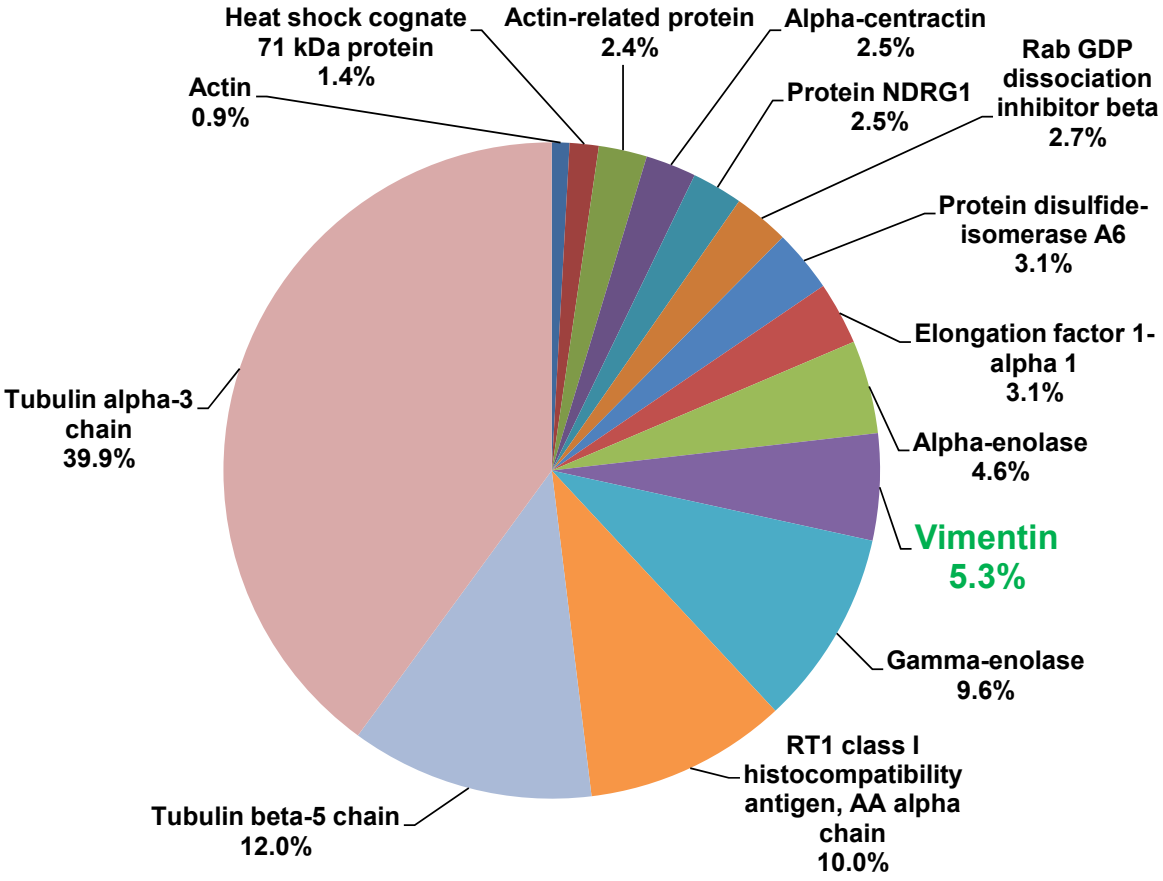

Fig 5.14A. Composition of ~48 kDa L6MP protein band, as determined by LC-MS/MS. Values are expressed as percent relative abundance of each protein as calculated by MS2-based spectral count method.

On the other hand, the ~55 kDa L6MP band primarily consists of vimentin (58.1%) followed by protein disulfide-isomerase (P04785; 26.9%) and caveolae-associated protein 1 (UniProt ID P85125; 15.0%) (Fig 5.14B). However, NnPLA$_2$-I bound L6MP and RP-HPLC purified L6RP1 was composed of 89.2% (Fig 5.14C) and 100% vimentin (P31000), respectively (Table 5.7).

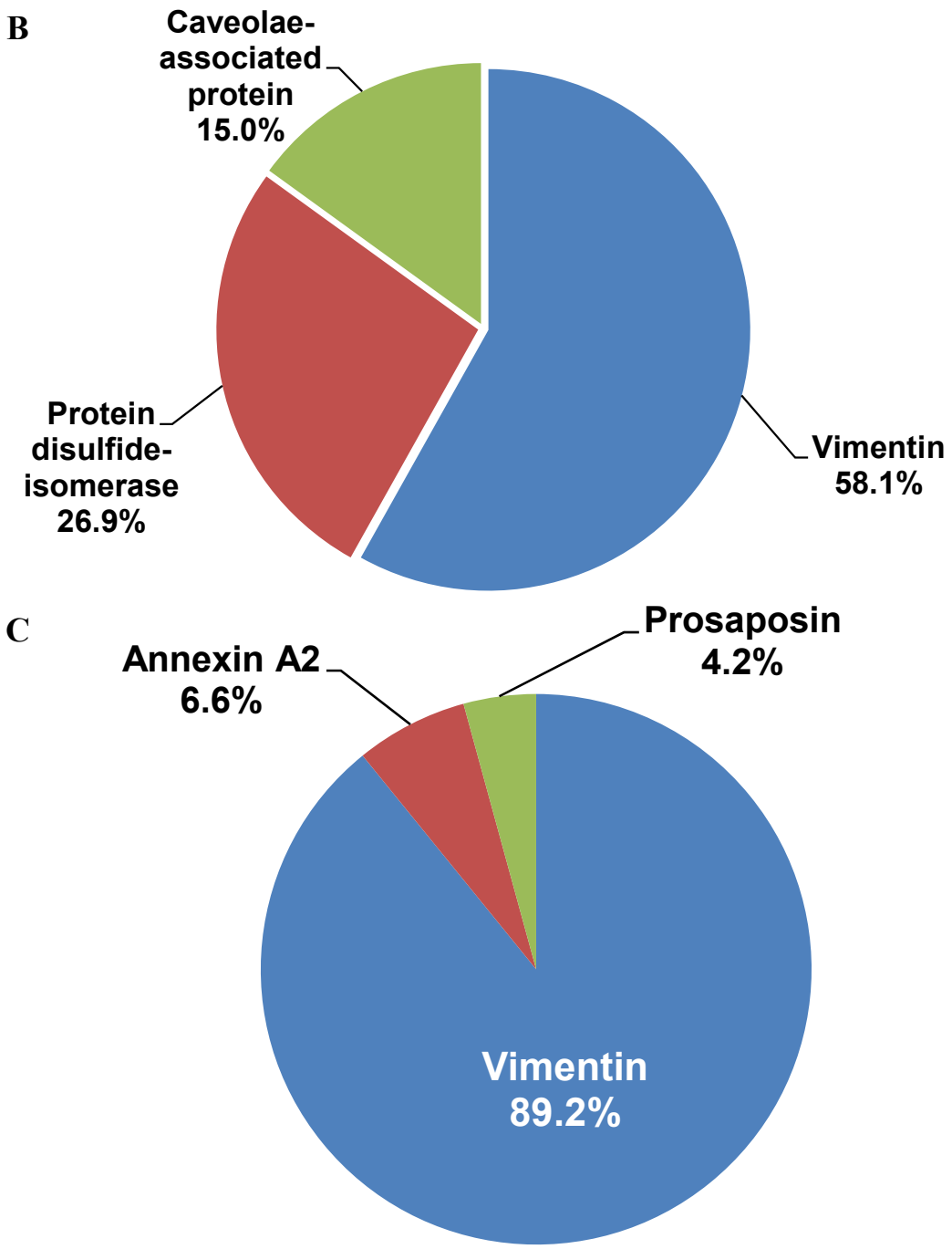

Fig 5.14. Composition of B. ~55 kDa L6MP protein band and C. affinity purified L6MP as determined by LC-MS/MS. Values are expressed as percent relative abundance of each protein as calculated by MS2-based spectral count method.

Table 5.7. Sequence alignment of LC-MS/MS identified tryptic peptides of affinity-purified NnPLA$_2$-I bound L6MP (blue), ~55 kDa L6MP band (red), ~48 kDa L6MP band (green), and vimentin P31000 from *Rattus norvegicus* (black). The

protein alignment was done using Clustal Omega programme (https://www.ebi.ac.uk/Tools/msa/clustalo/).

Source	Sequence alignment
NnPLA$_2$-I bound L6MP	----SVSSSSYR-MFGGSGTSSR----------TYSLGSALRPSTSRSLYSSSPGGAYVTR----
55 kDa protein band	----SVSSSSYR-MFGGSGTSSR----------TYSLGSALRPSTSRSLYSSSPGGAYVTR----
48 kDa protein band	----------SLYSSSPGGAYVTR----
Vimentin (P31000)	MSTRSVSSSSYRRMFGGSGTSSRPSSNRSYVTTSTRTYSLGSALRPSTSRSLYSSSPGGAYVTRSSAV
	:::::::: :::::::::: :::::::::::::**********
NnPLA$_2$-I bound L6MP	---SSMPGVRLLQDSVDFSLADAINTEFK----------FANYIDK---------ILLAELE
54 kDa protein band	----------FANYIDK---------ILLAELE
48 kDa protein band	---SSMPGVRLLQDSVDFSLADAINTEFK----------FANYIDKVR-------ILLAELE
Vimentin (P31000)	RLRSSMPGVRLLQDSVDFSLADAINTEFKNTRTNEKVELQELNDRFANYIDKVRFLEQQNKILLAELE
	:::::::::::::::::::::::::: ******:: *******
NnPLA$_2$-I bound L6MP	QLKGQGK----------QVDQLTNDK--VEVERDNLAEDIMR----------EEAESTLQ
54 kDa protein band	QLKGQGK--LGDLYEEEM----------DNLAEDIMR----LQEEMLQREEAESTLQ
48 kDa protein band	QLKGQGKSRLGDLYEEEMR---RQVDQLTNDKARVEVERDNLAEDIMR----LQEEMLQREEAESTLQ
Vimentin (P31000)	QLKGQGKSRLGDLYEEEMRELRRQVDQLTNDKARVEVERDNLAEDIMRLREKLQEEMLQREEAESTLQ
	******* ::::::::: ::::::::: :::::********* ::::::::********
NnPLA$_2$-I bound L6MP	SFRQDVDNASLAR----------KLHDEEIQELQAQIQEQHVQIDVDVSKPDLTAALRDV
54 kDa protein band	SFR----------KVESLQEEIAFLK----------
48 kDa protein band	SFRQDVDNASLAR-----KVESLQEEIAFLKKLHDEEIQELQAQIQEQHVQIDVDVSKPDLTAALR--
Vimentin (P31000)	SFRQDVDNASLARLDLERKVESLQEEIAFLKKLHDEEIQELQAQIQEQHVQIDVDVSKPDLTAALRDV
	***:::::::::: ::
NnPLA$_2$-I bound L6MP	RQQYESVAAK----------FADLSEAANR----------QVQSLTCEVDALK------
54 kDa protein band	----------FADLSEAANR----------
48 kDa protein band	----------FADLSEAANRNNDALR----------QVQSLTCEVDALKGTNESL
Vimentin (P31000)	RQQYESVAAKNLQEAEEWYKSKFADLSEAANRNNDALRQAKQESNEYRRQVQSLTCEVDALKGTNESL
	:::::::::: ********** :::::: ::::::::::::
NnPLA$_2$-I bound L6MP	-----EMEENFALEAANYQDTIGR----------
54 kDa protein band	-----EMEENFALEAANYQDTIGRLQDEIQNMKEEMAR----------
48 kDa protein band	ER---EMEENFALEAANYQDTIGRLQDEIQNMKEEMAR----------
Vimentin (P31000)	ERQMREMEENFALEAANYQDTIGRLQDEIQNMKEEMARHLREYQDLLNVKMALDIEIATYRKLLEGEE
	:: ********** ::::::::::::::
NnPLA$_2$-I bound L6MP	--ISLPLPNFSSLNLRETNLESLPLVDTHSK----------DGQVINETSQHHDDLE
54 kDa protein band	----------ETNLESLPLVDTHSK----------DGQVINETSQHHDDLE
48 kDa protein band	--ISLPLPNFSSLNLRETNLESLPLVDTHSKR----------DGQVINETSQHHDDLE
Vimentin (P31000)	SRISLPLPNFSSLNLRETNLESLPLVDTHSKRTLLIKTVETRDGQVINETSQHHDDLE
	:::::::::::::********** **********

(*) represents identical residues in all sequences; (:) represents identical residues in at least one sequences with respect to P31000

5.2.18 Spectrofluorometry analysis to determine binding of NnPLA$_2$-I and its cognate complex to vimentin

5.2.18.1 Dose- and time-dependent binding of NnPLA$_2$-I to vimentin

Increasing concentration of NnPLA$_2$-I led to a corresponding decrease in fluorescence intensity of vimentin suggesting protein–protein interactions leading to quenching of aromatic residues of vimentin (Figs 5.15A). A saturation in binding with vimentin was observed at a 0.35 µM concentration of NnPLA$_2$-I (Fig 5.15A inset) and

the optimum time for $NnPLA_2$-I-vimentin binding was observed at 15 min post incubation of interacting proteins (Fig 5.15B).

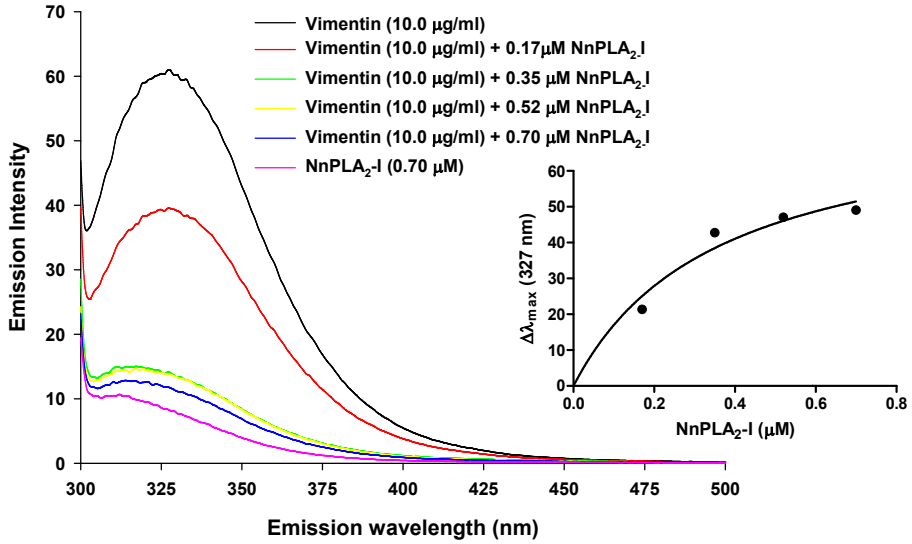

Fig 5.15A. Spectrofluorometry analysis to determine dose-dependent (0.17 – 0.70 µM) binding of $NnPLA_2$-I to vimentin (10.0 µg/ml). The reaction mixture was excited at 280 nm and the emission intensity was recorded from 300 – 500 nm. The values are mean of triplicate determinations.

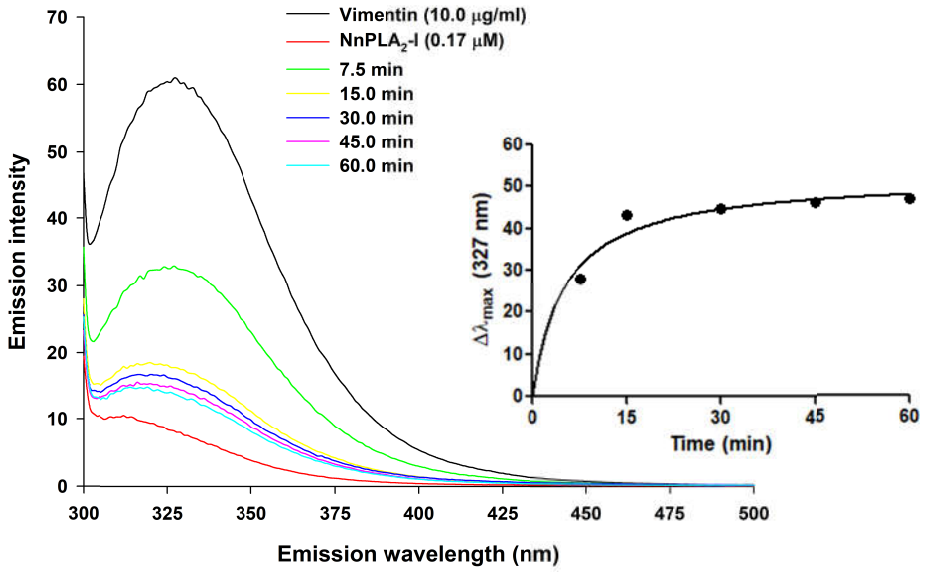

Fig 5.15B. Spectrofluorometry analysis to determine time-dependent (7.5 – 60 min) binding of $NnPLA_2$-I (0.17 µM) to vimentin (10.0 µg/ml). The reaction mixture was

excited at 280 nm and the emission intensity was recorded from 300 – 500 nm. The values are mean of triplicate determinations.

5.2.18.2 Dose- and time-dependent binding of $NnPLA_2$-I cognate complex to vimentin

Similar to $NnPLA_2$-I, increasing concentration of $NnPLA_2$-I cognate complex led to decrease in fluorescence of vimentin (Fig 5.16A). However, in a sharp contrast to $NnPLA_2$-I, the cognate complex at a concentration of 25.0 µg/ml (containing 0.70 µM of $NnPLA_2$-I) did not show saturation of binding with vimentin (Fig 5.16A inset). The optimum time of binding of $NnPLA_2$-I cognate complex with vimentin was observed 45 min post incubation (Fig 5.16B).

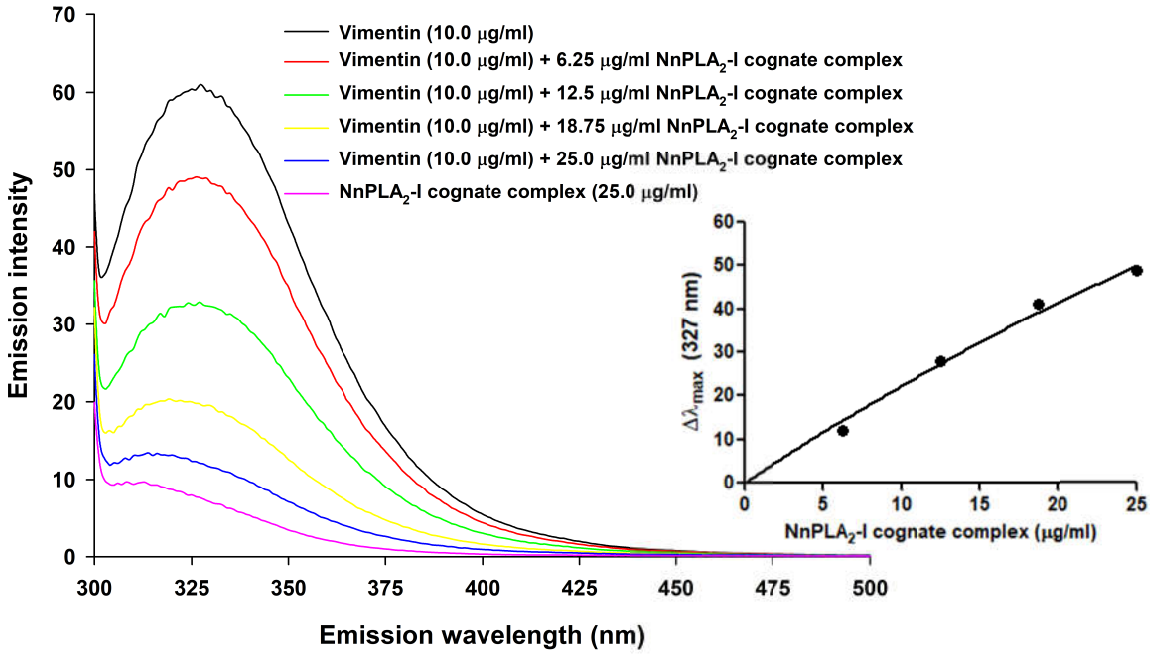

Fig 5.16A. Spectrofluorometry analysis to determine dose-dependent (6.25 – 25.0 µg/ml) binding of $NnPLA_2$-I to vimentin (10.0 µg/ml). The reaction mixture was excited at 280 nm and the emission intensity was recorded from 300 – 500 nm. The values are mean of triplicate determinations.

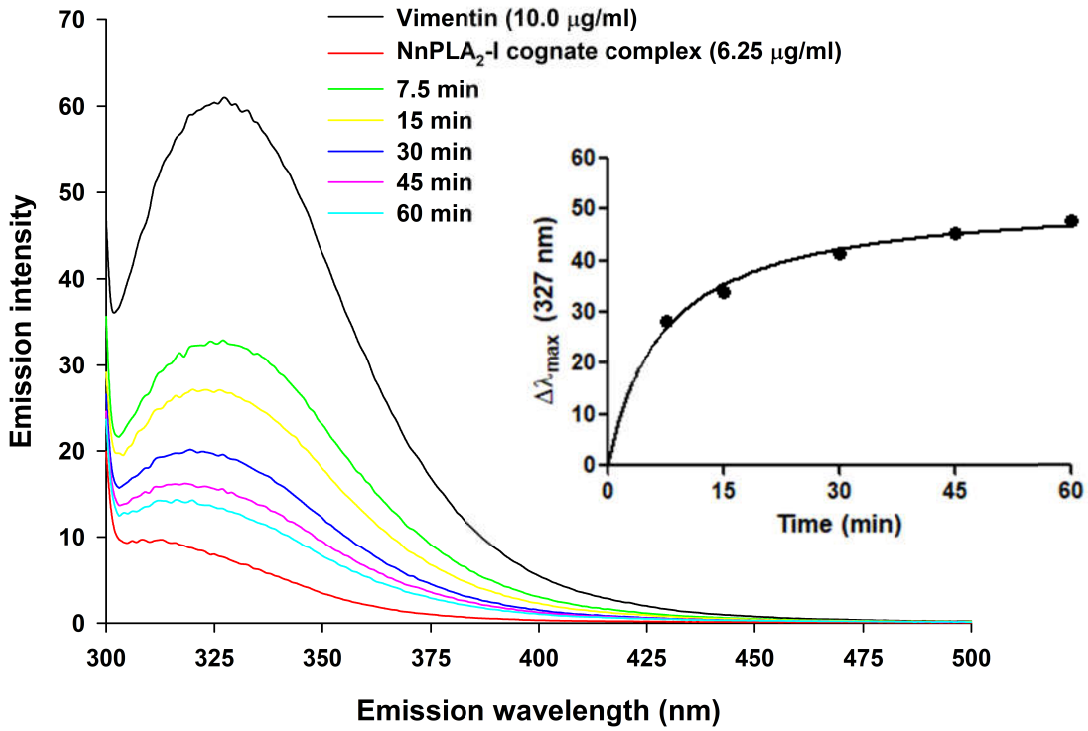

Fig 5.16B. Spectrofluorometry analysis to determine time-dependent (7.5 – 60 min) binding of NnPLA$_2$-I (6.25 µg/ml containing 0.17 µM of NnPLA$_2$-I) to vimentin (10.0 µg/ml). The reaction mixture was excited at 280 nm and the emission intensity was recorded from 300 – 500 nm. The values are mean of triplicate determinations.

5.2.19 *In silico* analysis to demonstrate binding of NnPLA$_2$-I and its cognate complex to the rod region of vimentin

5.2.19.1 Docking of NnPLA$_2$-I with different chains of vimentin

The interaction between the different regions of vimentin (as receptor) and NnPLA$_2$-I (as ligand) was predicted to be strong and stable with predicted binding free energy (ΔG) and dissociation constant (K_D) values of -12.86 kcal/mol and 3.67 × 10^{-10} M, respectively. The best predicted structure of NnPLA$_2$-I (chapter IV, Fig 4.20) showed interaction with all the four chains (PDB IDs 3s4rB, 3uf1A, 3trtA, and 1gk4D) of vimentin with negative global energy; the highest binding was noted with 3s4rB followed by 3trtA chains (Table 5.8).

Table 5.8. A comparison of the global energy of binding of $NnPLA_2$-I to different regions of rod structure of vimentin. The global energy values were predicted using Firedock server and the types of interactions were determined using PDBsum server.

Vimentin (chain PDB ID)	Amino acid region	Global energy	Non-bonded contacts	Hydrogen bonds	Salt bridges
3s4rB	99 – 189	-111.04	120	12	4
3uf1A	146 – 249	-82.55	86	8	0
3trtA	261 – 335	-107.58	147	12	2
1gk4D	330 – 407	-100.68	156	7	0

PDBsum analysis of the $NnPLA_2$-I – 3s4rB model (Fig 5.17A, panels I,II) showed that 19 residues of $NnPLA_2$-I interacted with 15 residues of 3s4rB via 120 non-bonded contacts, 12 H-bonds, and 4 salt bridges suggesting strong affinity between the these two proteins (Fig 5.17A, panel III; Table 5.8). Nevertheless, 22 residues of $NnPLA_2$-I interacted with 3trtA region of vimentin (15 residues) by 147 non-bonded contacts, 12 H-bonds and 2 salt bridges (Fig 5.17B, Table 5.8). Interestingly, the Asp48 residue of $NnPLA_2$-I has been predicted to be involved in salt bridge and / or H-bonds formation with the two regions of vimentin (panel III of Figs 5.17A,B). The $NnPLA_2$-I also showed binding to 3uf1A (Fig 5.17C) and 1gk4D (Fig 5.17D) regions of vimentin via non-bonded contacts and H-bonds; however, this binding strength was determined to be less as compared to that of 3s4rB and 3trtA regions (Table 5.8).

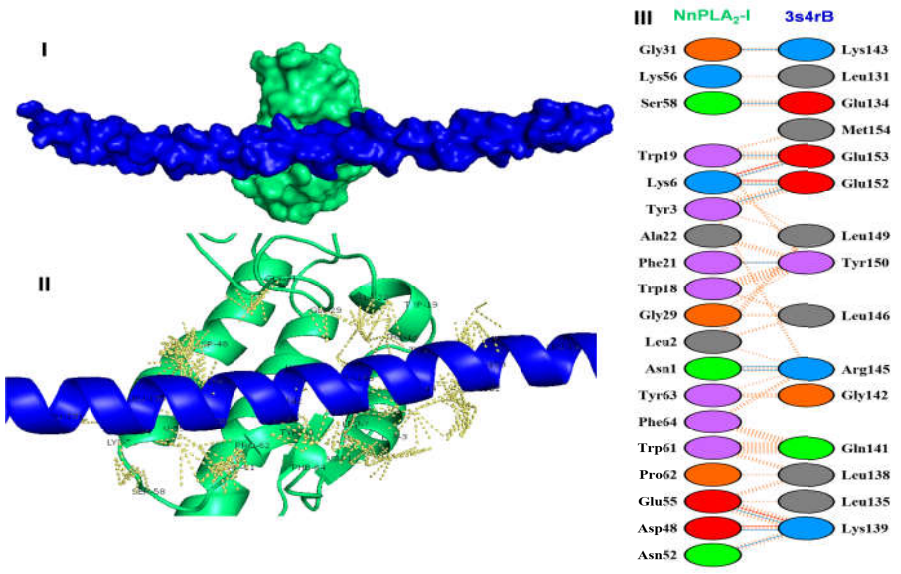

Fig 5.17A. Most favorable docking model of interaction of $NnPLA_2$-I (green chain) with 3s4rB chain (blue chain) of vimentin as predicted by ClusPro 2.0 server and refined by Firedock server. The model has been visualized using PyMol software.

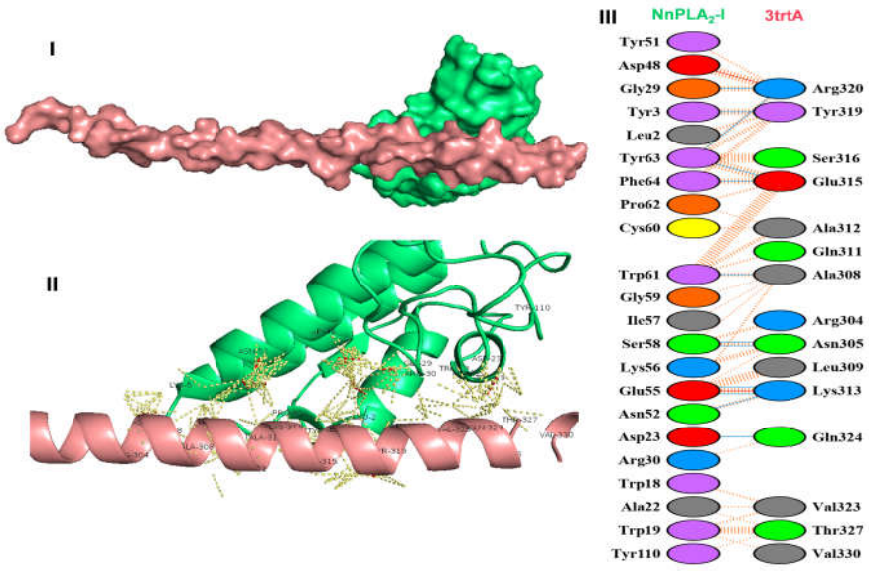

Fig 5.17B. Most favorable docking model of interaction of $NnPLA_2$-I (green chain) with 3trtA chain (pink chain) of vimentin as predicted by ClusPro 2.0 server and refined by Firedock server. The model has been visualized using PyMol software.

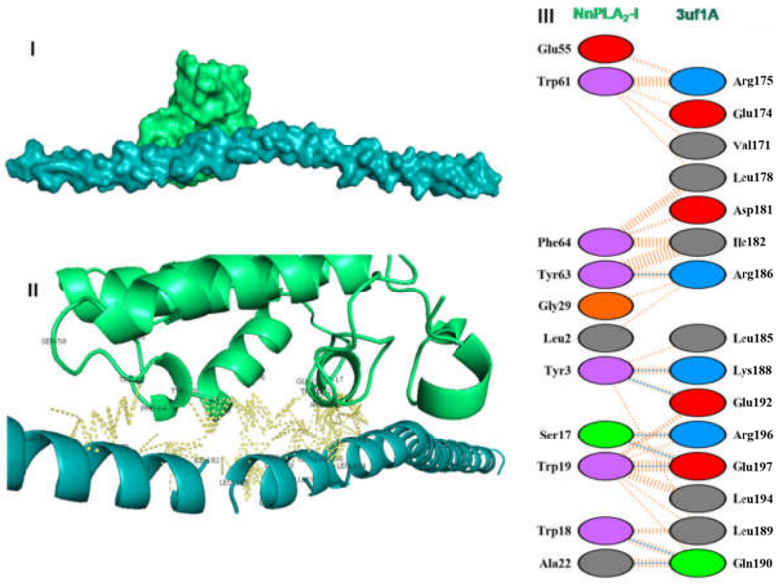

Fig 5.17C. Most favorable docking model of interaction of $NnPLA_2$-I (green chain) with 3uf1A chain (teal chain) of vimentin as predicted by ClusPro 2.0 server and refined by Firedock server. The model has been visualized using PyMol software.

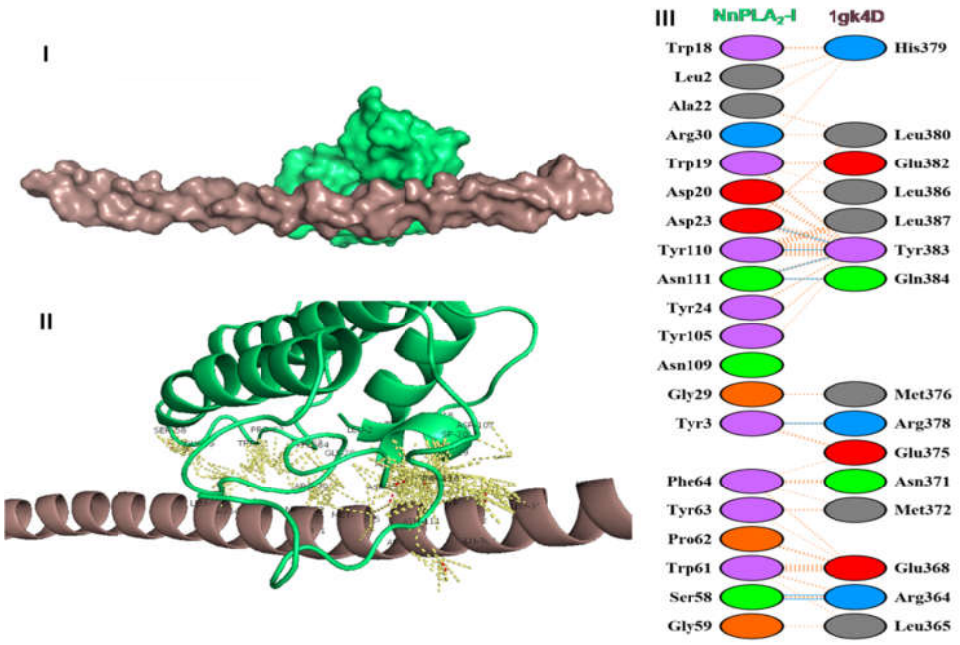

Fig 5.17D. Most favorable docking model of interaction of $NnPLA_2$-I (green chain) with 1gk4D chain chain (brown chain) of vimentin as predicted by ClusPro 2.0 server and refined by Firedock server. The model has been visualized using PyMol software.

5.2.19.2 Docking of CTx, LNTx, and NGF with vimentin

The CTx, LNTx, and NGF showed significant interaction (negative global energies) with 3s4rB (Fig 5.18) and 3trtA (Fig 5.19) chains of vimentin via non-bonded contacts, H-bonds, and salt bridges. The binding energies of docking of each of these proteins with vimentin are summarized in Table 5.9.

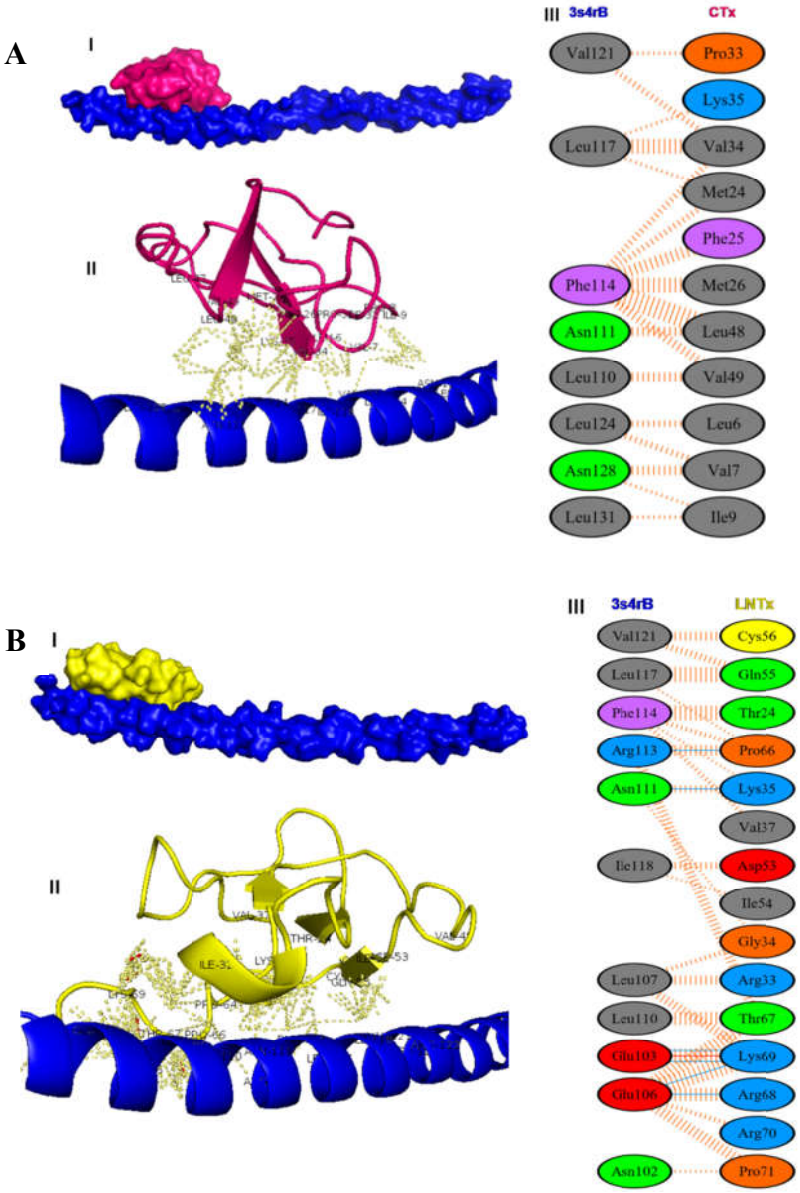

Fig 5.18. ClusPro 2.0 and Firedock predicted best docking models of 3s4rB chain of vimentin with A. CTx and B. LNTx. The docking has been shown as surface models **(I)**, ribbon models with surface interactions **(II),** and residue-to-residue

interactions between the two chains as predicted by PDBSum software **(III)**. The surface and ribbon models were visualized using PyMol software

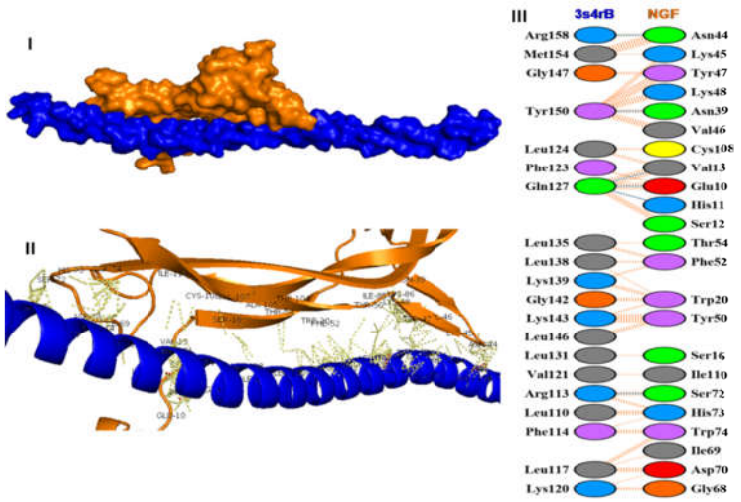

Fig 5.18C. ClusPro 2.0 and Firedock predicted best docking models of 3s4rB chain of vimentin with NGF. The docking has been shown as surface model **(I)**, ribbon model with surface interactions **(II)**, and residue-to-residue interactions between the two chains as predicted by PDBSum software **(III)**. The surface and ribbon models were visualized using PyMol software.

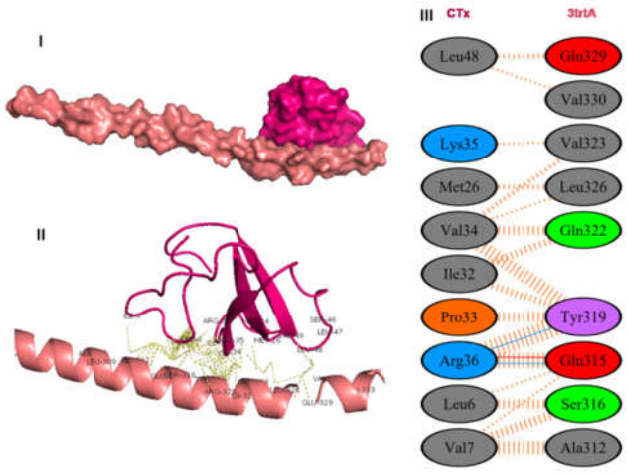

Fig 5.19A. ClusPro 2.0 and Firedock predicted best docking models of 3trtA chain of vimentin with CTx. The docking has been shown as surface model **(I)**, ribbon model with surface interaction **(II)**, and residue-to-residue interactions between the two chains as predicted by PDBSum software **(III)**. The surface and ribbon models were visualized using PyMol software.

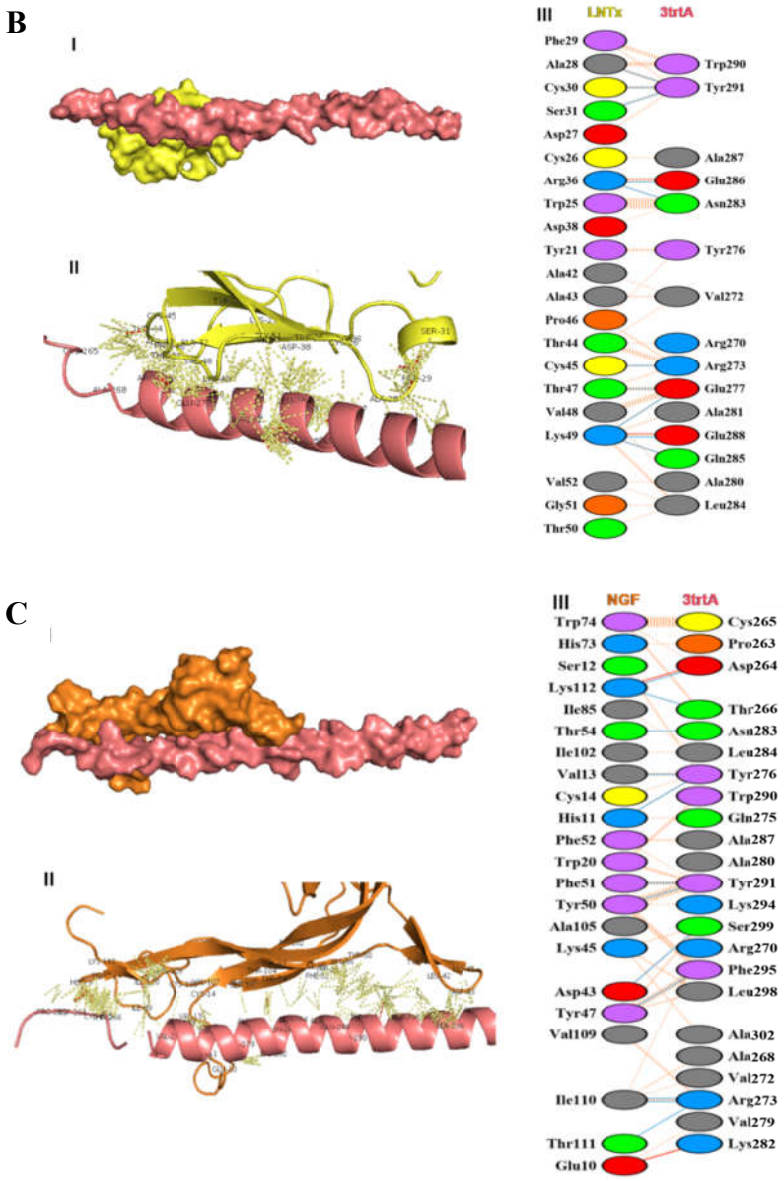

Fig 5.19. ClusPro 2.0 and Firedock predicted best docking models of 3trtA chain of vimentin with B. LNTx and C. NGF. The docking has been shown as surface models **(I)**, ribbon models with surface interactions **(II)**, and residue-to-residue interactions between the two chains as predicted by PDBSum software **(III)**. The surface and ribbon models were visualized using PyMol software.

5.2.19.3 Docking of NnPLA$_2$-I with CTx, LNTx, and NGF to form a cognate complex

The *in silico* analysis showed that NnPLA$_2$-I forms a stable complex with 3FTxs and NGF of NnV (Fig 5.20) with negative global energy (Table 5.9).

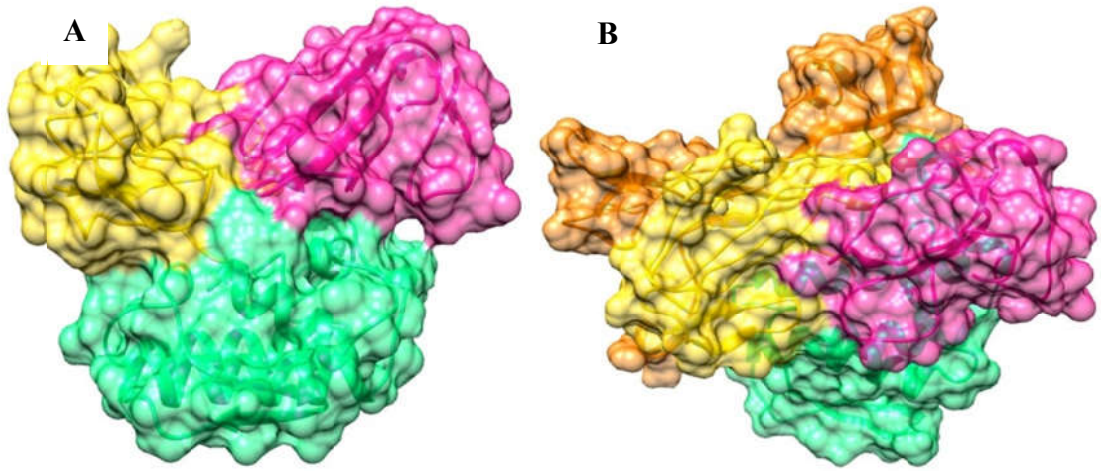

Fig 5.20. ClusPro 2.0 and Firedock predicted best models of A. $NnPLA_2$-I – CTx – LNTx and B. $NnPLA_2$-I – CTx – LNTx – NGF interactions. $NnPLA_2$-I, CTx, LNTx, and NGF are represented by green, pink, yellow, and orange coloured ribbon / surface models, respectively. The surface and ribbon models were visualized using UCSF Chimera software.

Table 5.9. A comparison of the global energy of binding of the components of $NnPLA_2$-I cognate complex to two regions of the rod structure of vimentin. 3s4rB (rod region; 99 – 189) and 3trtA (rod region; 261 – 335). The global energy values were predicted using Firedock server.

Protein	Global energy of complex	Global energy of interaction with 3s4rB region of vimentin	Global energy of interaction with 3trtA region of vimentin
$NnPLA_2$-I	-	-111.04	-107.58
CTx	-	-114.77	-101.74
LNTx	-	-90.12	-84.55
NGF	-	-125.62	-132.73
$NnPLA_2$-I-CTx	-111.55	-104.28	-97.63
$NnPLA_2$-I-LNTx	-123.37	-104.43	-94.14
$NnPLA_2$-I-NGF	-136.94	-131.94	-107.42
$NnPLA_2$-I-CTx-	-91.30	-109.69	-95.61

LNTx			
$NnPLA_2$-I-CTx-LNTx-NGF	-174.54	-138.20	-113.19

5.2.19.4 Docking of 3FTx-$NnPLA_2$-I and 3FTx-NGF-$NnPLA_2$-I complexes with vimentin

Although individual components of $NnPLA_2$-I-cognate complex showed binding to 3s4rB and 3trtA chains of vimentin (Figs 5.18, 5.19) albeit the 3FTx-$NnPLA_2$-I complex showed slightly lower binding efficiency to 3s4rB (Fig 5.21A) and 3trtA (Fig 5.21B) chains as compared to binding to these regions by individual $NnPLA_2$-I (Table 5.8). In this complex, only $NnPLA_2$-I showed binding to 3s4rB region of vimentin via 94 non-bonded contacts, 6 H-bonds, and 3 salt bridges (Fig 5.21A). The PDBsum server did not predict direct interactions between 3FTxs of the cognate complex and 3s4rB region of vimentin (Fig 5.21A). However, both $NnPLA_2$-I and LNTx interacted with 3trtA region of vimentin via non-bonded contacts (88 and 49, respectively) and H-bonds (4 and 2, respectively) (Fig 5.21B).

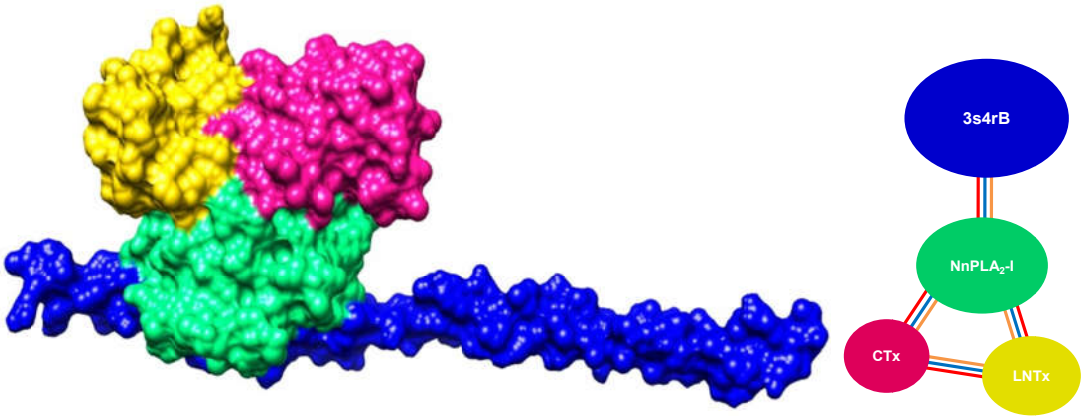

Fig 5.21A. Best docking model of $NnPLA_2$-I-3FTx complex with 3s4rB chain of vimentin. The model (left panel) has been visualized using PyMol software. Right panel of the figure shows schematic representation of interaction of each component of the cognate complex with vimentin; orange, blue and red lines represent non-bonded contacts, H-bonds and salt bridges, respectively.

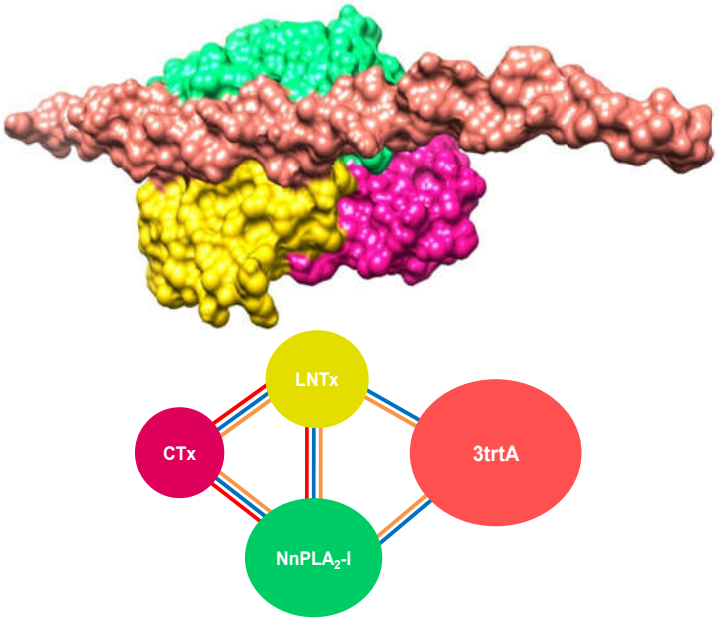

Fig 5.21B. Best docking model of $NnPLA_2$-I-3FTx complex with 3trtA chain of vimentin. The model (left panel) has been visualized using PyMol software. Right panel of the figure shows schematic representation of interaction of each component of the cognate complex with vimentin; orange, blue and red lines represent non-bonded contacts, H-bonds and salt bridges, respectively.

On the other hand, the $NnPLA_2$-I-3FTx-NGF complex showed higher binding to both 3s4rB and 3trtA regions of vimentin (Table 5.9). In the complex, both $NnPLA_2$-I and NGF showed binding to 3s4rB region of vimentin via non-bonded contacts (94 and 48, respectively), H-bonds (6 and 3, respectively), and salt bridges (3 each) (Fig 5.22A, Table 5.10).

Similar interactions were predicted for the interaction between $NnPLA_2$-I cognate complex and 3trtA region of vimentin (Table 5.9). It was observed that $NnPLA_2$-I interacted with vimentin via 118 non-bonded contacts, 7 H-bonds and 2 salt bridges, whereas NGF interacted with 3trtA region of vimentin through 35 non-bonded contacts, 4 H-bonds and 1 salt bridge (Fig 5.22B, Table 5.10). The presence of NGF in the complex, therefore, may enhance the binding with vimentin which corroborates well with the *in vitro* results.

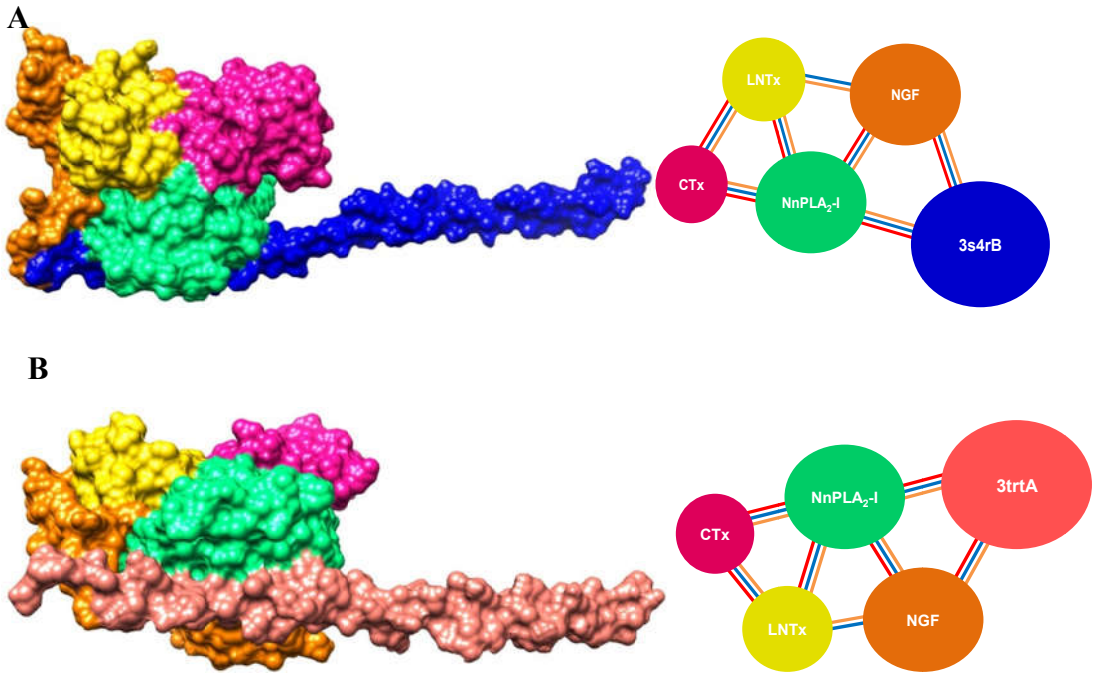

Fig 5.22. Best docking model of $NnPLA_2$-I-3FTx-NGF complex with A. 3s4rB and B. 3trtA chains of vimentin. All models have been visualized using PyMol software. Right panel of the figure shows schematic representation of interaction of each component of the cognate complex with vimentin; orange, blue and red lines represent non-bonded contacts, H-bonds and salt bridges, respectively.

Table 5.10. A comparison of the interactions between the components of $NnPLA_2$-I – 3FTx – NGF cognate complex and 3s4rB (99 – 189) region of vimentin. The interactions were predicted by PDBSum software.

Interacting proteins (A-B)	No. of residues involved (A:B)	Interface area (Å) (A:B)	No. of bonds		
			Non-bonded	H-bond	Salt bridge
$NnPLA_2$-I – 3s4rB	19:14	847:888	94	6	3
NGF – 3s4rB	3:5	240:195	48	3	3
$NnPLA_2$-I – LNTx	23:12	828:999	141	9	3
$NnPLA_2$-I – CTx	10:10	495:489	93	5	1
$NnPLA_2$-I – NGF	19:20	912:772	154	13	1

LNTx – CTx	11:9	485:535	48	3	1
LNTx – NGF	20:26	974:951	121	8	0

Table 5.11. A comparison of the interactions between the components of $NnPLA_2$-I – 3FTx – NGF cognate complex and 3trtA (261 – 335) region of vimentin. The interactions were predicted by PDBSum software.

Interacting proteins (A-B)	No. of residues involved (A:B)	Interface area (Å) (A:B)	No. of bonds		
			Non-bonded	H-bond	Salt bridge
$NnPLA_2$-I – 3trtA	19:10	687:768	118	7	2
NGF – 3trtA	4:7	225:214	35	4	1
$NnPLA_2$-I – LNTx	24:12	846:1018	153	10	3
$NnPLA_2$-I – CTx	10:10	502:495	93	5	1
$NnPLA_2$-I – NGF	20:20	954:822	147	11	1
LNTx – CTx	11:8	483:537	44	3	1
LNTx – NGF	21:26	985:972	131	10	0

5.2.20 ELISA to determine $NnPLA_2$-I does not bind to tail region of vimentin

ELISA result demonstrated that pre-incubation of vimentin with anti-vimentin monoclonal antibodies against the tail region of vimentin did not affect the binding of $NnPLA_2$-I or its cognate complex to vimentin (Fig 5.23), suggesting that $NnPLA_2$-I binds to vimentin other than its tail region. However, due to unavailability of commercial monoclonal antibodies against the rod and head regions of vimentin, the interaction of $NnPLA_2$-I with the rod region of vimentin could not be further confirmed by *in vitro* analysis.

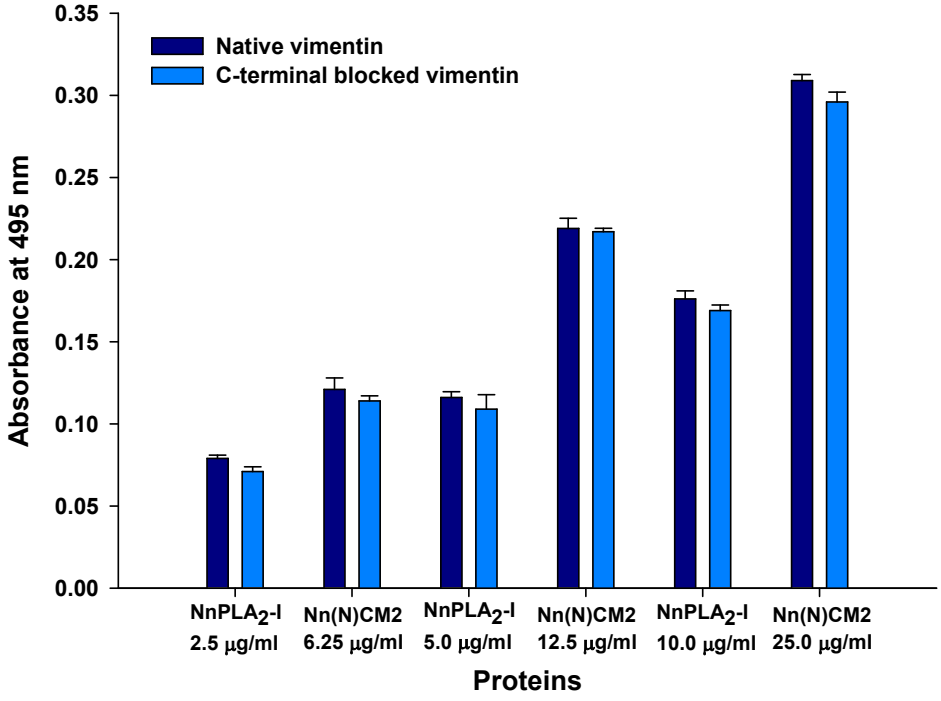

Fig 5.23. ELISA showing binding of $NnPLA_2$-I to native and tail-blocked vimentin. Vimentin was pre-incubated with anti-vimentin antibodies raised against the tail region to block the C-terminal of the protein. Binding of $NnPLA_2$-I was detected by anti-$NnPLA_2$-I polyclonal antibodies (primary) and HRP-conjugated anti-rabbit IgG secondary antibodies. Values are mean ± SD of triplicate determinations.

5.3 Discussion

Toxin synergism, a fascinating phenomenon to enhance toxicity of interacting components has been well documented in many different snake venoms, albeit this phenomenon is poorly investigated and understood to date [24-27]. The LC-MS/MS analysis of NnV separated by 2D SDS-PAGE under reduced and non-reduced conditions unambiguously demonstrated the formation of $NnPLA_2$-I-3FTxs-NGF cognate complex, may be by weak non-covalent interactions among the components of cognate complex [28,29]. As the term suggests, 'cognate' refers to 'related' or 'connected'. Since the precise stoichiometry of each individual component in the complex was not determined, the complex was named as an $NnPLA_2$-I cognate complex.

The significant enhancement of cytotoxicity of $NnPLA_2$-I as a component of the cognate complex compared to individual $NnPLA_2$-I is evident from the facts that – (a) $NnPLA_2$-I alone cannot induce cytotoxicity in partially differentiated rat myoblasts, and (b) neutralization with anti-$NnPLA_2$-I antibodies or alkylation of His48 active site of $NnPLA_2$-I significantly reduced the cytotoxic effect of $NnPLA_2$-I cognate complex. This result is in accordance with previous reports demonstrating several snake venom toxins tend to form a stable or cognate complex of higher molecular mass that significantly potentiate their cytotoxicity and pharmacological property against target cells and / or organisms [23,28,30-32]. It has also been well documented that cytotoxins and neurotoxins from cobra venom can form a stable cognate complex with the catalytically active PLA_2s from the same venom [25,26,29,33,34]; however, this binding may not enhance the catalytic activity of PLA_2 enzyme which is according to a previous observation from our laboratory [29]. Therefore, it is not surprising that $NnPLA_2$-I cognate complex would show a significantly higher cytotoxicity as compared to individual components of the complex. Further, partially differentiated rat myoblast are of mesenchymal origin and a significantly higher cytotoxicity of $NnPLA_2$-I cognate complex on this cell suggests the probable pathophysiological role of this complex in cobra venom-induced myopathy and muscular damage [35-37]. However, the other pathophysiological function(s) of this complex in cobra bite patients, if any, remains to be explored.

The cognate complex of $NnPLA_2$-I showed significantly higher cytotoxicity in myogenic cells as compared to other mammalian cells. Several factors including phospholipids composition of the target cell membrane, cholesterol / phospholipids ratio, physicochemical properties of a membrane, and / or presence of a specific toxin receptor in the cell surface may play an important role in snake venom-induced membrane damage and / or cytotoxicity [16,17,25,26]. $NnPLA_2$-I demonstrates preferential binding to phosphatidylcholine (PC) as compared to phosphatidylethanolamine (PE) or phosphatidylserine (PS) (Figs 4.22A,B, section 4.2.9.2, chapter IV). The differential composition of PC as well as occurrence of a large number of PLA_2-sensitive PC domain in the outer plasma membrane of the treated mammalian cells may explain the higher cytotoxicity of $NnPLA_2$-I and / or its cognate complex towards rat myogenic cells compared to other mammalian cells [12,25].

Further, the PLA_2-interacting cobra venom neurotoxins are also reported to display cell-specific cytotoxicity on mammalian cells [25] which further supports the differential cytotoxicity of $NnPLA_2$-I-cognate complex on mammalian cells. Furthermore, $NnPLA_2$-I and its cognate complex cannot show antibacterial activity due to absence of PC and low number of PLA_2 sensitive phospholipid (PE) domains on the outer membrane of bacterial cells [11,12].

It has been well documented that snake venom PLA_2s bind to certain phospholipid micro-domains of cell membranes that acts as a platform for PLA_2 adhesion and catalysis leading to cellular disintegration [10,12]; nevertheless, only few studies have shown the binding of snake venom PLA_2s to protein receptor(s) present on outer surface of cell membrane [38-42]. Further, except for plasma membrane bound nucleolin [42], there is dearth of knowledge regarding the consequence or pathophysiological significance of interaction / binding of snake venom PLA_2 to other cell surface receptors / acceptors. The present study suggests a high affinity binding of $NnPLA_2$-I to a ~55 kDa protein acceptor, vimentin, present in outer membrane of rat myoblasts and this binding as well as cytotoxicity against the myoblasts was significantly enhanced when $NnPLA_2$-I exists in a cognate complex. Cobra venom cytotoxins and PLA_2-interacting neurotoxins have been shown to kill the cells by non-selectively disrupting the cell membranes [25,26,33,34]. These reports corroborate well with the present study showing $NnPLA_2$-I cognate complex also retains a part of its cytotoxicity after treatment with anti-PLA_2 antibodies or alkylation of His-48 of $NnPLA_2$-I with *p*-BPB. Therefore, it may be anticipated that after binding with rat myoblasts, the cytotoxin and neurotoxin components of the cognate complex first destabilize the phospholipids bilayer of the target cell membranes that leads to higher binding of PLA_2 on dislocated and disorganized phospholipids bilayer of myoblasts resulting in a significantly higher ($p < 0.01$) membrane damage and cell death by $NnPLA_2$-I-cognate complex compared to individual $NnPLA_2$-I or 3FTxs [26,29,33].

Studies have shown a synergism between PLA_2s and 3FTxs [25,26,29,31,33,34]; however, their exact mechanism of pathophysiological function in complex form remains to be explored. Another component of the $NnPLA_2$-I complex was determined to be an NGF which is one of the most fascinating proteins found in cobra venom

[43,44]. The presence of NGF significantly enhanced the cytoxicity of the cognate complex. Although non-toxic in isolation [44], this class of proteins in association with other venom toxins is known to elicit severe toxicity against different cell lines [43]. Owing to its specificity towards vimentin, it may be anticipated that cobra venom PLA_2 and / or 3FTxs employ NGF as a carrier to specific target sites [43,45] to enhance the toxicity of the cognate complex. This phenomenon reinstates the effect of toxin synergism wherein the presence of even a trace quantity of one or more venom toxin potentiates the effect of other venom proteins [23,32]. Nevertheless, further characterization of each individual component of cognate complex is necessary to study their exact stoichiometry of interactions to form a stable complex [23] as well as to explore their definite role in binding with membrane lipids and / or proteins.

In 1990, Lambeau and colleagues [41] demonstrated the high affinity binding of a high molecular weight (180 kDa) monomeric membrane protein in rabbit myotubes to a PLA_2 from *Oxyuranus scutellatus* venom; however, the exact pathophysiological significance of PLA_2-membrane protein interaction was unknown. Another Lys49 myotoxic PLA_2 from venom of *Agkistrodon piscivorus piscivorus* was shown to bind to a kinase insert domain containing receptor (KDR) [13,40]. However, such interactions may not always demonstrate a functional relevance in the pathophysiology exhibited by the snake venom PLA_2 enzymes [46]. Recently, it has been demonstrated that a myotoxic Lys49 PLA_2 (Mt-II) from *Bothrops asper* binds to membrane-bound nucleolin at low temperatures [42]. However, at physiological temperature, this binding was followed by internalization and co-localization of Mt-II and nucleolin in paranuclear and nuclear areas of myotubes showing the role of this association in myotoxicity exhibited by the PLA_2 [42].

Vimentin is a type III intermediate filament (IF) protein of the cytoskeleton known to be constitutively expressed in mesenchymal cells [47] and is mainly involved in tissue integrity [48,49]. Vimentin serves as a target for human group IIA (hGIIa) PLA_2 enzyme to enhance the binding of the latter to activated T-cells in inflamed synovium of rheumatoid arthritis patients [50]. Further, hGIIa internalizes and co-localizes with vimentin in rheumatoid fibroblast-like synoviocytes [51] which indicates the association of PLA_2 with vimentin in a pathophysiological process. Vimentin is also

one of the fifteen proteins that interacted and co-localized with *Bothrops asper* Lys49 myotoxin II (Mt-II) in C2C12 myotubes [42] thereby re-instating the involvement of such an interaction with pathophysiology of snakebite.

Vimentin is reported to be expressed on the surface of different cells such as apoptotic neutrophils, T cells [52], activated macrophages [53], vascular endothelial cells [54], skeletal muscle cells [55], and platelets [56] by some unknown mechanism or by post-translational modification of vimentin [57]. The involvement of cell surface vimentin in binding with several extracellular proteins, toxins, and microorganisms has been well documented [54,58,59]; nevertheless, this is the first report suggesting the role of membrane bound vimentin as a myogenic cell surface acceptor for NnV acidic PLA_2 enzyme. The binding with vimentin was found to be critical for initiation of infection and pathogenesis by the virulent strain of Japanese encephalitis virus [60] and the present study shows a crucial vimentin – *N. naja* venom PLA_2 interaction which may have a role in inducing cytotoxicity. Further, pre-incubation of cognate complex with polyvalent antivenom has shown to reduce its cytotoxicity towards rat myoblasts which advocates early antivenom therapy for successful management of cobra bite patients. Although it was expected that $NnPLA_2$-I and its cognate complex should also show binding to intracellular vimentin present in cytosolic proteins of partially differentiated rat myoblasts, however, our observation was quite contrary. Interference from other cytosolic proteins or specific conformational changes of cytosolic vimentin may influence this binding; nevertheless, extensive studies would be required to pin-point the differences in binding between membrane bound and cytosolic vimentin.

Vimentin is composed of three regions - a head, which initiates and direct the filament assembly; a rod region and a tail region [61]. The *in silico* analysis indicated that the rod region of vimentin may be involved in high affinity binding to $NnPLA_2$-I by a mechanism similar to the binding of dengue virus and *Clostridium botulinum* C3 exoenzyme to the rod region of vimentin present in outer surface of vascular endothelial cells and hippocampal HT22 cells, respectively [54,62]. $NnPLA_2$-I internalization in myoblasts may be associated to its binding with vimentin in a manner similar to vimentin mediated uptake of C3 exoenzyme to hippocampal HT22 cells [59,62].

Further, the *in silico* study has provided a strong evidence of higher binding of $NnPLA_2$-I-cognate complex to vimentin compared to individual $NnPLA_2$-I.

Thus, the enhanced binding and toxicity of $NnPLA_2$-I-3FTx cognate complex as compared to individual $NnPLA_2$-I sheds light on the possible role of vimentin as a cellular acceptor in cobra venom PLA_2 complexes induced cytotoxicity. Further, the in-sufficient neutralization of the cytotoxic property of the cognate complex demonstrated by commercial polyvalent anti-snake venom raises concern regarding successful hospital management of cobra bite patients.

Bibliography

[1] Mukherjee, A. K. A major phospholipase A_2 from *Daboia russelii russelii* venom shows potent anticoagulant action via thrombin inhibition and binding with plasma phospholipids. *Biochimie*, 99: 153-161, 2014.

[2] Saikia, D. and Mukherjee, A. K. Anticoagulant and membrane damaging properties of snake venom phospholipase A_2 enzymes. In Gopalakrishnakone P., Inagaki H., Vogel CW., Mukherjee A., Rahmy T., editors, *Snake Venoms, Toxinology*, pages 87-104. Springer, Dordrecht, 2017.

[3] Condrea, E., Fletcher, J. E., Rapuano, B. E., Yang, C. C., and Rosenberg, P. Dissociation of enzymatic activity from lethality and pharmacological properties by carbamylation of lysines in *Naja nigricollis* and *Naja naja atra* snake venom phospholipases A_2. *Toxicon*, 19(5): 705-720, 1981.

[4] Kini, R. M. and Evans, H. J. Structure-function relationships of phospholipases. The anticoagulant region of phospholipases A_2. *Journal of Biological Chemistry*, 262(30): 14402-14407, 1987.

[5] Lomonte, B., Angulo, Y., and Calderon, L. An overview of lysine-49 phospholipase A_2 myotoxins from crotalid snake venoms and their structural determinants of myotoxic action. *Toxicon*, 42(8): 885-901, 2003.

[6] Kini, R. M. Excitement ahead: structure, function and mechanism of snake venom phospholipase A_2 enzymes. *Toxicon*, 42(8): 827-840, 2003.

[7] Osipov, A. V., Filkin, S. Y., Makarova, Y. V., Tsetlin, V. I., and Utkin, Y. N. A new type of thrombin inhibitor, noncytotoxic phospholipase A_2, from the *Naja haje* cobra venom. *Toxicon*, 55(2-3): 186-194, 2010.

[8] Hanasaki, K. and Arita, H. Phospholipase A_2 receptor: a regulator of biological functions of secretory phospholipase A_2. *Prostaglandins & Other Lipid Mediators*, 68-69: 71-82, 2002.

[9] Hanasaki, K. Mammalian phospholipase A_2: phospholipase A_2 receptor. *Biological & Pharmaceutical Bulletin*, 27(8): 1165-1167, 2004.

[10] Doley, R., King, G. F., and Mukherjee, A. K. Differential hydrolysis of erythrocyte and mitochondrial membrane phospholipids by two phospholipase A_2 isoenzymes (NK-PLA_2-I and NK-PLA_2-II) from the venom of the Indian monocled cobra *Naja kaouthia*. *Archives of Biochemistry and Biophysics*, 425(1): 1-13, 2004.

[11] Mukherjee, A. K. Correlation between the phospholipids domains of the target cell membrane and the extent of *Naja kaouthia* PLA_2-induced membrane damage: evidence of distinct catalytic and cytotoxic sites in PLA_2 molecules. *Biochimica et Biophysica Acta*, 1770(2): 187-195, 2007.

[12] Saikia, D., Bordoloi, N. K., Chattopadhyay, P., Choklingam, S., Ghosh, S. S., and Mukherjee, A. K. Differential mode of attack on membrane phospholipids by an acidic phospholipase A_2 (RVVA-PLA_2-I) from *Daboia russelli* venom. *Biochimica et Biophysica Acta (BBA)-Biomembranes*, 1818(12): 3149-3157, 2012.

[13] Montecucco, C., Gutierrez, J. M., and Lomonte, B. Cellular pathology induced by snake venom phospholipase A_2 myotoxins and neurotoxins: common aspects of their mechanisms of action. *Cellular and Molecular Life Sciences*, 65(18): 2897-2912, 2008.

[14] Ownby, C. L. and Colberg, T. R. Classification of myonecrosis induced by snake venoms: venoms from the prairie rattlesnake (*Crotalus viridis viridis*), western

diamondback rattlesnake (*Crotalus atrox*) and the Indian cobra (*Naja naja naja*). *Toxicon*, 26(5): 459-474, 1988.

[15] Mukherjee, A. K. and Maity, C. R. Biochemical composition, lethality and pathophysiology of venom from two cobras- *Naja naja* and *N. kaouthia*. *Comparative Biochemistry and Physiology. Part B, Biochemistry & Molecular Biology*, 131(2): 125-132, 2002.

[16] Gutierrez, J. M. and Ownby, C. L. Skeletal muscle degeneration induced by venom phospholipases A_2: insights into the mechanisms of local and systemic myotoxicity. *Toxicon*, 42(8): 915-931, 2003.

[17] Ownby, C. L., Fletcher, J. E., and Colberg, T. R. Cardiotoxin 1 from cobra (*Naja naja atra*) venom causes necrosis of skeletal muscle *in vivo*. *Toxicon*, 31(6): 697-709, 1993.

[18] Kini, R. M. and Chan, Y. M. Accelerated evolution and molecular surface of venom phospholipase A_2 enzymes. *Journal of Molecular Evolution*, 48(2): 125-132, 1999.

[19] Lomonte, B., Moreno, E., Tarkowski, A., Hanson, L. A., and Maccarana, M. Neutralizing interaction between heparins and myotoxin II, a lysine 49 phospholipase A_2 from *Bothrops asper* snake venom. Identification of a heparin-binding and cytolytic toxin region by the use of synthetic peptides and molecular modeling. *Journal of Biological Chemistry*, 269(47): 29867-29873, 1994.

[20] Tonello, F. and Rigoni, M. Cellular mechanisms of action of snake phospholipase A_2 Toxins. In Gopalakrishnakone P., Inagaki H., Vogel CW., Mukherjee A., Rahmy T., editors, *Snake Venoms, Toxinology*, pages 9-65. Springer, Dordrecht, 2017.

[21] Gutierrez, J. M. and Lomonte, B. Phospholipases A_2: unveiling the secrets of a functionally versatile group of snake venom toxins. *Toxicon*, 62: 27-39, 2013.

[22] Dutta, S., Chanda, A., Kalita, B., Islam, T., Patra, A., and Mukherjee, A. K. Proteomic analysis to unravel the complex venom proteome of eastern India

Naja naja: Correlation of venom composition with its biochemical and pharmacological properties. *Journal of Proteomics*, 156: 29-39, 2017.

[23] Mukherjee, A. K., Dutta, S., Kalita, B., Jha, D. K., Deb, P., and Mackessy, S. P. Structural and functional characterization of complex formation between two Kunitz-type serine protease inhibitors from Russell's Viper venom. *Biochimie*, 128-129: 138-147, 2016.

[24] Montecucco, C. and Rossetto, O. On the quaternary structure of taipoxin and textilotoxin: the advantage of being multiple. *Toxicon*, 51(8): 1560-1562, 2008.

[25] Mukherjee, A. K. Phospholipase A_2-interacting weak neurotoxins from venom of monocled cobra *Naja kaouthia* display cell-specific cytotoxicity. *Toxicon*, 51(8): 1538-1543, 2008.

[26] Gasanov, S. E., Dagda, R. K., and Rael, E. D. Snake venom cytotoxins, phospholipase A_2s, and Zn^{2+}-dependent metalloproteinases: Mechanisms of action and pharmacological relevance. *Journal of Clinical Toxicology*, 4(1): 1000181, 2014.

[27] Laustsen, A. H. Toxin synergism in snake venoms. *Toxin Reviews*, 35(3-4): 165-170, 2016.

[28] Doley, R. and Kini, R. M. Protein complexes in snake venom. *Cellular and Molecular Life Sciences*, 66(17): 2851-2871, 2009.

[29] Mukherjee, A. K. Non-covalent interaction of phospholipase A_2 (PLA_2) and kaouthiotoxin (KTX) from venom of *Naja kaouthia* exhibits marked synergism to potentiate their cytotoxicity on target cells. *Journal of Venom Research*, 1: 37-42, 2010.

[30] Banerjee, Y., Mizuguchi, J., Iwanaga, S., and Kini, R. M. Hemextin AB complex, a unique anticoagulant protein complex from *Hemachatus haemachatus* (African Ringhals cobra) venom that inhibits clot initiation and factor VIIa activity. *Journal of Biological Chemistry*, 280(52): 42601-42611, 2005.

[31] Cintra-Francischinelli, M., Pizzo, P., Rodrigues-Simioni, L., Ponce-Soto, L. A., Rossetto, O., Lomonte, B., Gutierrez, J. M., Pozzan, T., and Montecucco, C. Calcium imaging of muscle cells treated with snake myotoxins reveals toxin synergism and presence of acceptors. *Cellular and Molecular Life Sciences*, 66(10): 1718-1728, 2009.

[32] Mukherjee, A. K. and Mackessy, S. P. Pharmacological properties and pathophysiological significance of a Kunitz-type protease inhibitor (Rusvikunin-II) and its protein complex (Rusvikunin complex) purified from *Daboia russelii russelii* venom. *Toxicon*, 89: 55-66, 2014.

[33] Gasanov, S., Kolusheva, S., Salakhutdinov, B., Beknazarov, U., and Aripov, T. The mechanism of cobra venom phospholipase A_2 and cytotoxin synergistic action on phospholipids membrane structure. *Dokl Akad Nauk UzSSR*: 44-46, 1991.

[34] Chaim-Matyas, A., Borkow, G., and Ovadia, M. Synergism between cytotoxin P4 from the snake venom of *Naja nigricollis nigricollis* and various phospholipases. *Comparative Biochemistry and Physiology Part B: Biochemistry and Molecular Biology*, 110(1): 83-89, 1995.

[35] Harris, J. B. and Cullen, M. J. Muscle necrosis caused by snake venoms and toxins. *Electron Microscopy Reviews*, 3(2): 183-211, 1990.

[36] Bawaskar, H. S., Bawaskar, P. H., Punde, D. P., Inamdar, M. K., Dongare, R. B., and Bhoite, R. R. Profile of snakebite envenoming in rural Maharashtra, India. *Journal of the Association of Physicians of India*, 56: 88-95, 2008.

[37] Kularatne, S. A., Budagoda, B. D., Gawarammana, I. B., and Kularatne, W. K. Epidemiology, clinical profile and management issues of cobra (*Naja naja*) bites in Sri Lanka: first authenticated case series. *Transactions of the Royal Society of Tropical Medicine and Hygiene*, 103(9): 924-930, 2009.

[38] Lambeau, G., Barhanin, J., and Lazdunski, M. Identification of different receptor types for toxic phospholipases A_2 in rabbit skeletal muscle. *FEBS Letters*, 293(1-2): 29-33, 1991.

[39] Lambeau, G., Ancian, P., Nicolas, J. P., Beiboer, S. H., Moinier, D., Verheij, H., and Lazdunski, M. Structural elements of secretory phospholipases A_2 involved in the binding to M-type receptors. *Journal of Biological Chemistry*, 270(10): 5534-5540, 1995.

[40] Yamazaki, Y., Matsunaga, Y., Nakano, Y., and Morita, T. Identification of vascular endothelial growth factor receptor-binding protein in the venom of eastern cottonmouth. A new role of snake venom myotoxic Lys49-phospholipase A_2. *Journal of Biological Chemistry*, 280(34): 29989-29992, 2005.

[41] Lambeau, G., Schmid-Alliana, A., Lazdunski, M., and Barhanin, J. Identification and purification of a very high affinity binding protein for toxic phospholipases A_2 in skeletal muscle. *Journal of Biological Chemistry*, 265(16): 9526-9532, 1990.

[42] Massimino, M. L., Simonato, M., Spolaore, B., Franchin, C., Arrigoni, G., Marin, O., Monturiol-Gross, L., Fernandez, J., Lomonte, B., and Tonello, F. Cell surface nucleolin interacts with and internalizes *Bothrops asper* Lys49 phospholipase A_2 and mediates its toxic activity. *Scientific Reports*, 8(1): 10619, 2018.

[43] Kostiza, T. and Meier, J. Nerve growth factors from snake venoms: chemical properties, mode of action and biological significance. *Toxicon*, 34(7): 787-806, 1996.

[44] Angeletti, R. H. Nerve growth factor from cobra venom. *Proceedings of the National Academy of Sciences of the United States of America*, 65(3): 668-674, 1970.

[45] Levi-Montalcini, R. The nerve growth factor: thirty-five years later. *Bioscience Reports*, 7(9): 681-699, 1987.

[46] Lomonte, B. and Rangel, J. Snake venom Lys49 myotoxins: From phospholipases A_2 to non-enzymatic membrane disruptors. *Toxicon*, 60(4): 520-530, 2012.

[47] Mani, S. A., Guo, W., Liao, M. J., Eaton, E. N., Ayyanan, A., Zhou, A. Y., Brooks, M., Reinhard, F., Zhang, C. C., Shipitsin, M., Campbell, L. L., Polyak, K., Brisken, C., Yang, J., and Weinberg, R. A. The epithelial-mesenchymal transition generates cells with properties of stem cells. *Cell*, 133(4): 704-715, 2008.

[48] Toivola, D. M., Tao, G. Z., Habtezion, A., Liao, J., and Omary, M. B. Cellular integrity plus: organelle-related and protein-targeting functions of intermediate filaments. *Trends in Cell Biology*, 15(11): 608-617, 2005.

[49] Eckes, B., Colucci-Guyon, E., Smola, H., Nodder, S., Babinet, C., Krieg, T., and Martin, P. Impaired wound healing in embryonic and adult mice lacking vimentin. *Journal of Cell Science*, 113(13): 2455-2462, 2000.

[50] Boilard, E., Bourgoin, S. G., Bernatchez, C., and Surette, M. E. Identification of an autoantigen on the surface of apoptotic human T cells as a new protein interacting with inflammatory group IIA phospholipase A_2. *Blood*, 102(8): 2901-2909, 2003.

[51] Lee, L. K., Bryant, K. J., Bouveret, R., Lei, P.-W., Duff, A. P., Harrop, S. J., Huang, E. P., Harvey, R. P., Gelb, M. H., and Gray, P. P. Selective inhibition of human group IIA secreted phospholipase A_2 (hGIIA) signaling reveals arachidonic acid metabolism is associated with colocalization of hGIIA to vimentin in rheumatoid synoviocytes. *Journal of Biological Chemistry*. M112: 397893, 2013.

[52] Moisan, E. and Girard, D. Cell surface expression of intermediate filament proteins vimentin and lamin B1 in human neutrophil spontaneous apoptosis. *Journal of Leukocyte Biology*, 79(3): 489-498, 2006.

[53] Mor-Vaknin, N., Punturieri, A., Sitwala, K., and Markovitz, D. M. Vimentin is secreted by activated macrophages. *Nature Cell Biology*, 5(1): 59-63, 2003.

[54] Yang, J., Zou, L., Yang, Y., Yuan, J., Hu, Z., Liu, H., Peng, H., Shang, W., Zhang, X., Zhu, J., and Rao, X. Superficial vimentin mediates DENV-2 infection of vascular endothelial cells. *Scientific Reports*, 6: 38372, 2016.

[55] Bryant, A. E., Bayer, C. R., Huntington, J. D., and Stevens, D. L. Group A streptococcal myonecrosis: increased vimentin expression after skeletal-muscle injury mediates the binding of *Streptococcus pyogenes*. *Journal of Infectious Diseases*, 193(12): 1685-1692, 2006.

[56] Podor, T. J., Singh, D., Chindemi, P., Foulon, D. M., McKelvie, R., Weitz, J. I., Austin, R., Boudreau, G., and Davies, R. Vimentin exposed on activated platelets and platelet microparticles localizes vitronectin and plasminogen activator inhibitor complexes on their surface. *Journal of Biological Chemistry*, 277(9): 7529-7539, 2002.

[57] Frescas, D., Roux, C. M., Aygun-Sunar, S., Gleiberman, A. S., Krasnov, P., Kurnasov, O. V., Strom, E., Virtuoso, L. P., Wrobel, M., and Osterman, A. L. Senescent cells expose and secrete an oxidized form of membrane-bound vimentin as revealed by a natural polyreactive antibody. *Proceedings of the National Academy of Sciences*: 201614661, 2017.

[58] Shigyo, M., Kuboyama, T., Sawai, Y., Tada-Umezaki, M., and Tohda, C. Extracellular vimentin interacts with insulin-like growth factor 1 receptor to promote axonal growth. *Scientific Reports*, 5: 12055, 2015.

[59] Adolf, A., Leondaritis, G., Rohrbeck, A., Eickholt, B. J., Just, I., Ahnert-Hilger, G., and Holtje, M. The intermediate filament protein vimentin is essential for axonotrophic effects of *Clostridium botulinum* C3 exoenzyme. *Journal of Neurochemistry*, 139(2): 234-244, 2016.

[60] Liang, J. J., Yu, C. Y., Liao, C. L., and Lin, Y. L. Vimentin binding is critical for infection by the virulent strain of Japanese encephalitis virus. *Cellular Microbiology*, 13(9): 1358-1370, 2011.

[61] Herrmann, H., Häner, M., Brettel, M., Müller, S. A., Goldie, K. N., Fedtke, B., Lustig, A., Franke, W. W., and Aebi, U. Structure and assembly properties of the intermediate filament protein vimentin: the role of its head, rod and tail domains. *Journal of Molecular Biology*, 264(5): 933-953, 1996.

[62] Rohrbeck, A., Schroder, A., Hagemann, S., Pich, A., Holtje, M., Ahnert-Hilger, G., and Just, I. Vimentin mediates uptake of C3 exoenzyme. *PloS One*, 9(6): e101071, 2014.